

A Generalized Biomass Pyrolysis Model Based on Superimposed Cellulose, Hemicellulose and Lignin Kinetics

R. S. MILLER and J. BELLAN *Jet Propulsion Laboratory, California Institute of Technology, Pasadena, CA 91109-8099*

(submitted June 14, 1996)

ABSTRACT-The pyrolysis of general biomass materials is modeled via a superposition of cellulose, hemicellulose and lignin kinetics. All three of the primary biomass components are modeled with multi-step kinetics involving both competitive primary pyrolysis and secondary tar decomposition reactions. Only "typical" (untreated) feedstocks are considered at atmospheric pyrolysis pressures. The kinetics scheme is then coupled to the porous particle model of Miller and Bellan (1996) along with appropriate properties and heats of reaction to provide a complete model for the pyrolysis of arbitrary biomass feedstocks and sample sizes. Comparisons with past isothermal and thermogravimetry experiments for a variety of biomass materials under both kinetically controlled and diffusion limited conditions show favorable agreement with the model predictions. In addition, discussions are provided which support the use of competitive char production kinetics over single and successive reaction schemes which cannot currently be reconciled with observed pyrolysis behavior.

Key words: biomass, modeling, porous particle, pyrolysis, wood

NOMENCLATURE

| | |
|------|-----------------------------------|
| A | Frequency constant. |
| C | Specific heat. |
| cl | Characteristic pore length scale. |
| D | Molecular species diffusivity. |
| e | Specific internal energy. |
| E | Activation energy. |
| K | Reaction rate. |
| m | Sample mass. |
| M | Molecular weight. |
| N | Total number of species. |
| p | Pressure. |
| r | Radial coordinate. |
| R | Radial position. |

| | |
|-----------|--|
| \bar{R} | Universal gas constant. |
| \dot{S} | Reaction source/sink term. |
| t | Time. |
| T | Temperature. |
| u | Gas phase velocity. |
| X | Char formation mass ratio for reaction K_3 , |
| Y | Gas phase mass fraction. |

Greek Symbols

| | |
|--------------|-----------------------------|
| Δh | Heat of reaction. |
| ϵ | Porosity. |
| div | Divergence of the velocity. |
| λ | Thermal conductivity. |
| μ | Molecular viscosity. |
| ρ | Apparent density. |
| $\hat{\rho}$ | True density. |
| σ | Stefan-Boltzmann constant. |
| w | Emissivity. |

Subscripts and Superscripts

| | |
|---------|---|
| 0 | Initial value. |
| eff | Effective. |
| f | Final. |
| g | Gas phase. |
| i | Species i . |
| j | Reaction j . |
| R | Reactor. |
| s | Solid phase. |
| t | Total (all species and phases). |
| T | Thermal. |
| v | constant Volume. |
| β | Component β ; cellulose, hemicellulose or lignin. |
| l | Excluding char |

1 INTRODUCTION

Biomass pyrolysis involves the heating of raw biomass or organic waste materials in the absence of an oxidizer in order to extract reaction products for later applications. The majority of early research in these fields focused on low temperature/low heating rate pyrolysis aimed at maximizing char yields for the production of charcoal fuel (Antal, 1982). However, interest in adhesive, resin and clean burning hydrogen fuel production has motivated research in the area of high temperature/high heating rate pyrolysis. These conditions are aimed at maximizing tar and gas yields while simultaneously minimizing char formation (e.g. Antal, 1982; DiBlasi, 1993b). Optimal pyrolysis conditions for various applications remain largely uncertain and accurate mathematical models are needed to aid in the design of scalable and efficient biomass conversion reactors (Dicbold and Power, 1988). Unfortunately, extensive investigations have not yielded a satisfactory pyrolysis model capable of predicting even bulk product yields obtained over wide ranges of pyrolysis conditions and for varying biomass feedstocks (Miller and Bellan, 1996).

For the purposes of the current study, biomass pyrolysis models may be divided into two primary categories; micro- and macro-particle models. "Micro-particle" pyrolysis involves the thermal decomposition of biomass materials with sample sizes sufficiently small such that diffusion effects become negligible and the pyrolysis is kinetically controlled. Thus, micro-particles are desirable in experiments focusing on identification of kinetic schemes. Critical particle size estimates for kinetic control are generally $\sim 100-1000 \mu\text{m}$ and are observed to decrease with increasing pyrolysis temperatures (e.g. Simmons and Gentry, 1986; Scott et. al., 1988; Koufopoulos *et. al.*, 1989; DiBlasi, 1996; Miller and Bellan, 1996). Particles larger than the critical limit are characterized by relatively large diffusion effects which can strongly affect the pyrolysis evolution due to internal and external temperature gradients, thermal inertia due to heat capacity effects, and also temperature variations resulting from endothermic (or exothermic) reactions (Pyle and Zaror, 1984; Kothari and Antal, 1985; Simmons and Gentry, 1986; Koufopoulos *et. al.*, 1991; DiBlasi, 1993a; DiBlasi, 1993b; Miller and Bellan, 1996). The modeling of these "macro-particle" effects is inherently difficult and requires not only a viable kinetics scheme, but also a minimal knowledge of thermo-chemical properties in combination with a robust physical model of internal particle phenomena. Unfortunately, the grinding of biomass materials to micro-particle sizes is economically unfeasible and macro-particle models are necessary for the prediction of commercially relevant pyrolysis processes (Antal, 1982; Dicbold and Power, 1988).

1.1 Micro-Particles

A viable kinetics scheme for the pyrolysis of micro-particles of general biomass feedstocks must accurately predict: 1) temporal evolutions, 2) bulk product groups and quantitative yields, 3) yield variations with temperature and

heating conditions, and 4) product yield variations with biomass feedstock. Knowledge of temporal evolutions is necessary for reactor design as pyrolysis conversion times can vary from the order of weeks for charcoal production to the order of a second or less for flash pyrolysis at high temperatures (Kothari and Antal, 1985; Diebold and Power, 1988; Antal and Mok, 1990; Miller and Bellan, 1996). The products of pyrolysis are generally lumped into three categories; residual carbon rich non-volatiles (char), condensable high molecular weight vapors (tar) and remaining low molecular weight gas phase species (gas). Residual char mass predictions may be sufficient for charcoal production; however, knowledge of tar and gas yields is necessary for many pyrolysis applications (e.g. adhesives, resins, hydrogen, etc.) (Diebold and Power, 1988). The majority of direct experimental evidence reveals that final pyrolysis char yields from kinetically controlled biomass particles are decreasing functions of the pyrolysis temperature and vary for differing feedstocks (Scott and Piskorz, 1982; Lidén *et al.*, 1988; Scott *et al.*, 1988; Koufopoulos *et al.*, 1989; Antal and Mok, 1990; Koufopoulos *et al.*, 1991; Hallgren and Wanzl, 1992; Maschio *et al.*, 1992; Güell *et al.*, 1992). Similar observations have been made for the separated primary biomass components; cellulose (Shafiqzadeh *et al.*, 1979; Scott *et al.*, 1988; Koufopoulos *et al.*, 1991), hemicellulose and lignin (Koufopoulos *et al.*, 1989). Previous investigations additionally provide evidence that general biomass pyrolysis behaves as a superposition of the independent kinetics of the primary components (Ward and Braslaw, 1985; Evans and Milne, 1987; Maschio *et al.*, 1992); however, Evans and Milne (1987) note that this is not necessarily true when significant mineral content is added to the sample. It is therefore reasonable to assume that the varying compositions of hard woods, soft woods, grasses, etc. are related to observed yield variations, particularly for untreated samples (see e.g. Koufopoulos *et al.*, 1989; Hallgren and Wanzl, 1992; Mok *et al.*, 1992).

Although there is strong evidence to support the above mentioned product yield dependencies, many researchers attempt to model pyrolysis kinetics with single step, or successive reactions which may be adjusted to fit the results of particular experiments; however, these models have the disadvantage of predicting constant char and product yields for all temperatures (see Antal, 1982; DiBlasi, 1993b for reviews). For example, Ward and Braslaw (1985) present a combination of single step CIIUOSC, and successive reaction hemicellulose and lignin kinetics for the superposition modeling of biomass pyrolysis. This method predicts yield variations with feedstock, but does not predict variations with temperature. A similar study by Varhegyi and Antal (1989) compares single step, independent and successive reaction schemes for the pyrolysis modeling of both treated and untreated samples of cellulose, hemicellulose and bagasse. Although suggested pathways are provided for each feedstock, errors are in no case larger than 3.0%. This would appear to indicate that it is possible to fit a variety of kinetics schemes to a particular experiment, provided that there are a sufficient number of adjustable parameters. In addition, the results of Varhegyi and Antal (1989) suggest that both different kinetic schemes and/or parameters are necessary

for each heating rate, thermal pre-treatment (moisture removal) and mineral content studied. This variation of kinetics schemes and /or parameters with the conditions of the experiments invalidates the usefulness of the results as it does not provide confidence to use them for untested conditions. However, this is the rationale of kinetics schemes/parameters: once determined from a finite number of experiments, they can be used for all conditions without heating rate and other related dependencies.

Both of the aforementioned pyrolysis experiments (Ward and Braslaw, 1985; Varhegyi *et. al.*, 1989) were performed using thermogravimetry (TGA) with relatively slow heating rates ($\sim 10K/min$), hence the majority of pyrolysis occurs at low temperatures due to relatively long exposure times required to reach the higher temperatures. The exclusive use of low heating rate TGA experiments can therefore cause difficulties in distinguishing between the high and low temperature contributions to the pyrolysis. Kinetics derived from studies such as those listed above, generally predict large char yield. These predictions cannot be reconciled with the results of higher temperature pyrolysis experiments. For example, isothermal pyrolysis experiments for maple wood indicate that pyrolysis yields are reduced from $> 25\%$ to 4% as the reaction temperature is increased from $725K$ to $1075K$ (Scott *et. al.*, 1988). In contrast, the Ward and Braslaw model predicts a constant yield $> 40\%$ for all temperatures. An additional problem is related to Antal's reported variations in kinetic parameters with heating rate that are inconsistent with the employed Arrhenius reaction rate which by definition is only temperature and sample mass dependent. In fact, these variations in observed yields can be explained consistently with thermal history effects; *i.e.* the integrated effects of all temperatures experienced by the pyrolyzing sample during its thermal evolution (see e.g. Miller and Bellan, 1996). Furthermore, while evidence supports the role of mineral and moisture content in pyrolysis behavior (see also Evans and Milne, 1987), large tables of kinetic parameters for differing contents and reaction conditions have neither scientific or commercial value because they are not consistent with Arrhenius rates and they are not useful in making predictions for untested conditions.

There are currently two primary reaction pathway models employed for the description of observed char and product yield variations; competitive and secondary. The first model utilizes "competitive" reactions of the virgin matrix often with an initialization reaction step. These models are generally variations of the "Broido-Shafizadeh" model of cellulose pyrolysis appearing in a modified form in Bradbury *et. al.* (1979) (see DiBlasi, 1993b; Antal and Varhegyi, 1998 for complete reviews of related work), in these competitive reaction schemes, char variations are explained through two (or more) competing primary reactions; one which dominates at low temperatures and produces char, and a second producing condensable tar which dominates at higher temperatures. A similar scheme with three competitive reactions was recently compiled by DiBlasi (1992) and DiBlasi (1993a) by combining a modified version of the primary wood reaction suggested by Turner and Mann (1981) with competing secondary tar reactions to both char and gas. However, this model does not account for yield dependencies on feedstock.

Miller and Bellan (1996) recently evaluated both the modified and unmodified versions of this wood scheme by comparing their predictions with experimental results and concluded that neither version was capable of reproducing observed trends in char yields. Koufopoulos *et al.* (1991) recently proposed a similar scheme which combines both primary and secondary chars with competitive reactions but is also unable to account for feedstock variations. The most robust of recent competitive reactions schemes that accounts for feedstock variations is that of Koufopoulos *et al.* (1989) (KML) based on superimposed cellulose, hemicellulose and lignin kinetics. Although good agreement was observed with their own experiments, it will be shown that the KML scheme is inconsistent with several cellulose pyrolysis experiments and is also incompatible with high temperature pyrolysis behavior.

The second reaction pathway model is based on an assumed "secondary" char formation mechanism (Madonsky, 1964; Lewellan *et al.*, 1976) and has received renewed interest by Antal and co-workers (e.g. Varhegyi *et al.*, 1989; Mok *et al.*, 1992; Varhegyi *et al.*, 1994; Antal and Varhegyi, 1995). This type of model generally suggests that the primary biomass decomposition is through a single step first order Arrhenius reaction with negligible char formation. The char is then formed through secondary reactions between vapor products catalyzed by contact with the solid matrix. Purely secondary char production predicts negligible char yields *unless* either the sample size is sufficiently large, or vapor products remain in contact with the sample in order to allow for catalytic reactions. Inorganic minerals and moisture levels are interpreted as additional catalysts influencing the secondary reactions. While evidence is provided which may support such effects, the results of many of the above mentioned experiments cannot be readily reconciled with such pyrolysis pathways; these experiments utilize small particle sizes with co-flowing nitrogen streams which inhibit vapors from prolonged contact with the solid. For example, the experiments of Scott *et al.* (1988) reveal char yields as large as $\approx 5\%$ from cellulose and $> 25\%$ from maple wood for particle sizes of $\approx 120\mu\text{m}$. In addition, there are no currently proposed secondary schemes available which can account for the catalytic reactions in a manner consistent with observation. Such models will have to consider surface reactions and detailed analyses of pore geometries and contact areas, similar to models already in use for coal gasification (for a discussion see Miller and Bellan, 1996). However, current secondary char formation models are limited to tables of single and successive reaction parameters for varieties of pyrolysis conditions and feed stocks which predict constant char yields with temperature (e.g. Varhegyi *et al.*, 1989).

1.2 Macro-particles

Macro-particle pyrolysis modeling requires knowledge of both chemical and particle properties. It was recognized in relatively early studies that primary pyrolysis is typically endothermic (see Antal, 1982; DiBlasi, 1993b for reviews). Experimental measurements indicate endothermic primary biomass decomposition to tars and gases, while char formation and secondary tar reactions are exothermic (Pyle and Zaror, 1984; Curtis and Miller, 1988;

Koufopoulos *et. al.*, 1991). Temperature overshoots above the reactor conditions have been observed for macro-particle pyrolysis at low temperatures (high char yields) by Koufopoulos *et. al.*, 1991; Maschio *et. al.*, 1992; Mok *et. al.*, 1992. These overshoots are consistent with the competitive (exothermic) char formation mechanism. The literature also contains relatively widespread experimental measurements of various properties for both wood and pyrolysis products including; thermal conductivity, heat capacity, apparent density, porosity, emissivity, molecular weight, viscosity, and mass diffusivity (e.g. Kansa *et. al.*, 1977; SERI, 1979; Pyle and Zaror, 1984; Evans and Milne, 1987; Curtis and Miller, 1988; Magnaterra *et. al.*, 1992).

Many models have been proposed for macro-particle pyrolysis which are based on assumptions of either large or small particle Biot numbers and/or simplified particle dynamics (see DiBlasi, 1993b; Antal and Varhegyi, 1995 for recent reviews). However, there is a lack of robust particle models capable of predicting wide ranges of pyrolysis conditions. The model of Chan *et. al.* (1985) is based on a combination of fundamental derivation and empirical correlations. This model describes the interior particle pyrolysis evolution and the results compared favorably with experiments of Oregon lodgepole pine wood devolatilization. Another more recent model is that of DiBlasi (DiBlasi, 1992; DiBlasi, 1993a; DiBlasi, 1994; DiBlasi, 1996) which was used to simulate the macro-particle pyrolysis of both cellulose and wood using kinetic models described above. The particle model incorporates linear property variations with composition (from the virgin to the char values), employs the empirical Darcy's Law for momentum transport and is valid only within the particle (boundary conditions are modeled through diffusion/radiative heat transfer with the reactor conditions). The particle model of Miller and Bellan (1996) eliminated several constraints inherent in the DiBlasi model. In particular, full property variations are studied, the gas phase velocity is modeled using a transient momentum equation, and exterior thermal and mass boundary layers are included. A comparison with the DiBlasi model indicated that neglect of the thermal boundary layer exterior to the particle may lead to large over predictions of the particle surface temperature ($\sim 100K$ for reactor temperatures $\geq 1000K$). An evaluation of both the cellulose and wood kinetics used by DiBlasi revealed that while the cellulose model is in agreement with expected behavior and past experiments, the wood model over predicts char formation. Miller and Bellan (1996) also showed that pyrolysis occurs in three distinct regimes characterized by: 1) an initial heating period, 2) primary pyrolysis at a nearly constant "effective pyrolysis temperature" due to endothermicity, and 3) final heating and pyrolysis conclusion after the particle mass has become too small for endothermicity to balance thermal diffusion. These regimes are most easily distinguished when the reactor temperature is larger than the effective pyrolysis temperature ($\sim 650K$) and their prediction is indicative of the robustness of the model. These regimes are in agreement with the calculations of Narayan and Antal (1996) who interpreted the experimental results of Leck *et. al.* (1985) through a phase change analogy model, but they did not identify the three regimes. However, no macro-particle model has yet

been combined with kinetics, heats of reaction and properties yielding a model capable of predicting observed experimental pyrolysis behavior for general biomass feedstocks; particularly at high temperatures.

The objective of this paper is to present a complete model for the numerical simulation of macro-particle pyrolysis of general biomass feedstocks. The goal of the model is to predict the pyrolysis yields associated with "typical" biomass samples. Potential alterations necessary to account for mineral and moisture content and/or pressure are postponed for future work. A new micro-particle scheme based on superimposed cellulose, hemicellulose and lignin kinetics is first generated via an evaluation of three past experiments for lignin, maple and beech wood pyrolysis. The new kinetics are then incorporated into the previous porous particle model of Miller and Bellan (1996) together with appropriately compiled heats of reaction and properties. Detailed comparisons are made with a variety of past experiments of both micro- and macro-particle pyrolysis for many different feedstocks. Additional discussions are provided which address the issues of both competitive and single step or successive char production models. The paper is organized as follows: Section 2 discusses motivations for the current work. Section 3 presents the micro-particle kinetics along with discussions and comparisons with past experiments of sub-millimeter biomass particle pyrolysis. Section 4 introduces the macro-particle model and associated experimental comparisons. Section 5 is devoted to conclusions and further discussions.

2 MOTIVATION

The motivation for the development of a new kinetics scheme for general biomass pyrolysis is summarized by the results presented in Fig. 1. This figure compares the final char yield (final residual mass) from several experiments of isothermal wood pyrolysis with the values predicted by three previous kinetic models. The experimental results are for maple, oak, olive husk and poplar wood. The conditions under which these experiments, and all others considered in this work, are performed is provided in Table 1 and corresponding biomass compositions (cellulose, hemicellulose and lignin) are listed in Table 2. All of the experiments use co-flowing nitrogen streams to remove gaseous pyrolysis products (except Güell *et al.* who use hydrogen). In particular, note that the experiments of Scott *et al.* (1988) for maple pyrolysis (see Fig. 1), performed in a "cryovortactor," utilize very small particle sizes ($\approx 120 \mu\text{m}$). In addition, care was taken in Scott *et al.*'s experiments to insure that the total heatup time to the reactor conditions was less than approximately 10% of the total reaction time. This latter constraint aids in insuring that the majority of pyrolysis occurs at the reactor conditions, therefore minimizing the effects of the low temperature (high char) regime. It is therefore expected that the results of Scott *et al.*'s experiment provide an accurate assessment of high temperature pyrolysis behavior. The oak measurements are for similar particle sizes but for low temperatures which further dampen diffusion effects; however, the narrow range of temperatures employed limits any extrapolation of the observed behavior. No precise particle size is reported for either the

olive husk or poplar experiments, and it will be shown below that a macro-particle model is necessary for the correct description of these results. Nevertheless, the experimental results compiled in Fig. 1 clearly indicate the variation in pyrolysis product yields with both temperature and feedstock.

Three previous kinetic model predictions are also included in Fig. 1 and are indicated by the solid curves. The results predicted from the model developed herein are indicated by the dotted curve and will be discussed below. The compiled wood kinetics of DiBlasi with Turner and Mann's original parameters are represented by Curve #1. This model does not predict any effects of feedstock on yields, and additional problems have been discussed in detail in Miller and Bellan (1996); in particular, the modified DiBlasi kinetics predict char yields larger than 50% for all temperatures in this range. The kinetics of Ward and Braslaw (1985) are also included (Curve #2), as calibrated for the maple composition. This curve clearly reveals the problems associated with kinetics which do not predict yield variation with reactor temperature. The observed behavior is similar to the current capability of the secondary char production models. In these latter models, char yields can be functions of the feedstock, heating rate, mineral content and/or moisture content, but *not* temperature (e.g. Varhegyi *et al.*, 1989). Curve #3 is the KML model (also calibrated for maple) and is the most comprehensive of the three kinetics in that it is able to predict yield variations with *both* temperature and feedstock. The model was derived through an evaluation of both TGA and isothermal pyrolysis experiments for cellulose, hemicellulose and lignin, performed predominantly at relatively low reactor temperatures. This may explain the behavior observed in Fig. 1 in that relatively good agreement with the maple results is found only for temperatures below approximately 700 K. For temperatures over 1000 K, relative errors exceed 600%. The cause of this effect is illustrated in Fig. 2 which presents the char yields predicted by the KML model for the pure biomass components. Both the lignin and the hemicellulose models are observed to predict char yields larger than 20% for all temperatures. Given the relatively large mass fractions of these materials found in typical biomass (Table 2), the high temperature behavior of the KML model clearly requires modifications.

3 MICRO-PARTICLE MODEL

Several considerations must be addressed before proceeding with the development of a new kinetic model for biomass. Clearly, a model based on superimposed cellulose, hemicellulose and lignin is attractive due to its ability to predict variations in feedstock. Yield variations with temperature must also be incorporated into a robust kinetics. This rules out non-competitive schemes of the type available to date. The evidence discussed thus far is not conclusive as to the "true" mechanism for char production from pyrolysis (primary competitive vs. secondary catalytic); also, there is no irrefutable evidence available in the literature which shows that primary competitive mechanisms *cannot* account for observed behavior and associated mineral/moisture effects. In addition, the

interest in keeping the model relatively simple precludes a complicated analysis of surface reactions (particularly in the absence of precise porosimetry data, *i.e.* pore sizes and distributions) needed to finalize the secondary char production reaction mechanisms. These requirements therefore suggest the development of a compositional kinetics scheme based on primary competitive reactions, similar in form to the KML model, but additionally able to predict high temperature pyrolysis behavior.

A simple adjustment of the kinetic parameters of the KML scheme is not an option for the following reasons: The first problem with the KML scheme is illustrated in Fig.3 which depicts the final char yield from cellulose as a function of temperature from the isothermal experiments of Shafizadeh *et al.* (1979) and Scott *et al.* (1988) compared with the predicted yields from the kinetic model of KML and also from the cellulose model employed by DiBlasi (1994); DiBlasi (1996); Miller and Bellan (1996). The KML model is not able to predict the experimental cellulose pyrolysis behavior. This lack of agreement may be due in part to the use of cotton as a cellulose substitute in the KML experiments, Nevertheless, the disagreement is a liability for the current form of the KML scheme. Alternately, the single step cellulose model of Ward and Braslaw (1985) predicts a constant zero char yield from cellulose, while the scheme of Varhegyi *et al.* (1989) predicts a constant 7% yield from their standard cellulose experiment; thus, neither of these schemes is appropriate. The second problem with the KML scheme is the form of the hemicellulose kinetics which predicts a nearly constant char yield with temperature (see Fig.2); this is difficult to correct without relatively major changes to the current parameters. Third, the KML scheme employs a combination of a zeroth order initialization reaction followed by competitive reactions of order 1.5. Zeroth order reactions are not physically or mathematically self-consistent; they predict continuous and constant reaction rates unaltered by the changing particle composition and proceed through negative sample mass unless artificially halted by the numerical code.

3.1 Model Development

The above considerations lead to the following approach for developing the new biomass kinetics scheme: The cellulose kinetics outlined in DiBlasi (1994) is adopted due to a consideration of the results of Fig.3 and the previous validations of the scheme by DiBlasi (1994); DiBlasi (1996); Miller and Bellan (1996). Furthermore, the "skeleton" of the cellulose scheme is also used for the remaining biomass components; hemicellulose and lignin (Fig.4). The global use of this model simplifies both the analysis and the numerical implementation, The initialization reaction (K_1) does not produce any mass change and may be interpreted as a depolymerization step. During depolymerization, percentage change in the mass of the sample is small, however its composition may change substantially. This change in composition may also result in changes in physical properties, such as porosity. However, sample evolution during depolymerization has never been documented and compositional and

property changes are currently unknown. For simplicity, we limit all reactions to be Arrhenius;

$$K_j = A_j \exp \left[\frac{-E_j^\beta}{RT} \right], \quad (1)$$

irreversible and first order. The parameters for the secondary gas production (K_4) have already been documented in the above citations and are considered to be independent of the initial virgin matrix. Therefore, the only parameters requiring further specification are the rate constants (A_j^β), activation energies (E_j^β) and char production ratios (X^β) for the hemicellulose and lignin reactions.

In order to specify these parameters we begin with the rate constants and activation energies from Ward and Braslaw (1985) for the initialization steps of both species. The initial "guess" parameters for the competitive hemicellulose reactions are taken to be identical to the cellulose parameters due to their attractive behavior with temperature (see Figs. 2 and 3). Finally, the lignin parameters are taken from the KM 1, model, although instead of the original order 1.5 reactions, we assume first order reactions. The initial guess parameters for hemicellulose and lignin are iteratively adjusted using comparisons with the results of *only* three of the experiments (indicated by the superscript * in Table 1) in a zeroth order approximation we minimize the error with the maple pyrolysis experiments (Fig. 1) through small parameter adjustments in order to accurately capture the high temperature product yield variations. This step is not sufficient to quantify either the individual hemicellulose or lignin contributions, nor the rate constants governing the temporal pyrolysis evolution. To this end, a combination of the isothermal lignin pyrolysis experiments and the TGA decomposition of beech wood from Koufopoulos *et. al.* (1989) are considered. The kinetic parameters are modified to give best visual fit agreement with these experiments. The procedure is then repeated until a satisfactory total agreement is achieved. Extractives and/or ash content are included in the hemicellulose mass (Table 2) as this was found to provide the best overall results; this apportioning of extractives and ash was also used by Ward and Braslaw (1985) but differs from the even mass distribution between cellulose, hemicellulose and lignin chosen by Koufopoulos *et. al.* (1989).

The final model parameters are provided in Table 3 and the corresponding comparisons are given in Fig. 1 for maple yields, Fig. 5 for the temporal dependence of the residual mass from isothermal lignin pyrolysis and in Fig. 6 for the TGA experiments of beech wood. Temporal results for both the isothermal and TGA experiments are obtained from a finite difference numerical solution of the governing kinetics equations, whereas the final char yields in Fig. 7 are obtained analytically through the ratio of reaction rates $X K_3 / (K_2 + K_3)$. Results displayed in Fig. 5 show that the modeled prediction for the 873K lignin pyrolysis falls slightly below the corresponding data. This is acceptable due to uncertainties in the particle size (Table 1) and the associated possibility of diffusion effects when particles are large and/or reactor temperatures are high (Simmons and Gentry, 1986). Comparisons with the beech wood TGA experiments (Fig. 6) indicate a relatively good agreement with the temporal initialization and conclusion of the pyrolysis process. The qualitative effect of the heating rate is well captured; however,

the predicted magnitudes are slightly larger than observation at the 80K/min heating rate. This suggests that there may be some deficiencies associated with low temperature pyrolysis prediction (discussed in detail below). Since the original reference does not provide the actual experimental data and the points in Fig.6 were extracted from curve fits, no assessment of the experimental scatter is possible. We stress here that the finalized kinetic parameters in Table 3 were obtained using *only* the results of these three experiments. All further comparisons with experiments are performed completely *a posteriori*, without any readjustment of the parameters.

3.2 Kinetics Assessment

Several expected trends are incorporated in the model. One previous observation by Simmons and Gentry (1986) is that during biomass pyrolysis at relatively low temperatures, hemicellulose decomposes at nearly ten times the rate of cellulose. Furthermore, Antal and Varhegyi (1995) observe that hemicellulose decomposes at lower temperatures than cellulose, whereas lignin decomposes relatively slowly over a large range of temperatures. These observations are corroborated by Maschio *et al.* (1992) who report maximal pyrolysis rates (obtained from low heating rate TGA experiments) at approximately 640K for cellulose, 565K for hemicellulose and 620K for lignin. Results are obtained from the modeled kinetics (Table 3) by numerically simulating the conditions employed in Maschio *et al.*'s TGA experiments (101K/min heating rate). Figure 7 depicts these comparisons by showing the normalized particle mass rate of change as a function of temperature and can be compared to Fig.3 of Maschio *et al.* (1992). Important trends include: 1) a good qualitative agreement with the expected behavior for the pyrolysis ranges, and 2) good agreement with both the magnitude and the thermal location of the peak values for each curve. The primary deficiency observed in the results is that the biomass components begin their decompositions significantly later than the initialization temperatures observed in the experiment which were $\approx 475K$ for cellulose, $\approx 400K$ for hemicellulose and $\approx 450K$ for lignin. This disagreement is primarily responsible for the trends previously identified when discussing the TGA beech wood experiments of Fig.6. However, this has only a relatively small impact on the total mass conversion, even for slow heating rates in which significant time is spent in this regime. It will be shown that these effects are minimized for higher heating rates and/or reactor temperatures which are pertinent to commercial applications. In fact, the final char yields observed thus far for both the TGA of beech wood and the low temperature isothermal lignin decomposition are all in good agreement with the experimental measurements.

Before proceeding with comparisons of the model predictions with experimental results for various biomass feedstocks, it is informative to discuss the temperature variations of the predicted char yields for the three biomass components; this is illustrated in Fig.8. The model predicts that the char yield decreases monotonically with temperature for all components. In addition, lignin produces the largest char yields, cellulose produces the minimum, and hemicellulose yields are always bounded by the former two. These qualitative trends are in

agreement with past observations by Ward and Braslaw (1985); Koufopoulos *et al.* (1989); Varhegyi *et al.* (1989); Maschio *et al.* (1992) and lend credence to the model. Furthermore, the results of Fig.8 for the new kinetics can be compared directly to the predictions of the KMJ. model presented previously in Fig.2. There is a relatively good agreement between the predictions derived from the two models at relatively moderate temperatures near 700K. Below this range pyrolysis occurs extremely slowly and the yields produced at these temperatures are only significant in processes directed at char maximization (Antal and Mok, 1990). The largest differences in yield predictions occur in the high temperature regime. The new kinetic model is therefore expected to make its most significant contributions for high temperature/high heating rate pyrolysis aimed at gas and tar production.

A comparison of the model predictions with the oak pyrolysis experiments of Thurner and Mann (1981) is made in Fig.9. Although the reactor is held at a constant temperature ($T_R = 642K$), a thermo-couple embedded in the ceramic sample container revealed a strong temporal dependence of temperature during the initial stages of pyrolysis. A hyperbolic tangent function is used to model the reported thermal delay for the model simulation (compare to Fig.5 of the referenced work); however, the results are not very sensitive to the exact form of the delay. Furthermore, a co-flowing nitrogen stream used in the experiments carries away gaseous pyrolysis products to be rapidly cooled, thus inhibiting secondary vapor reactions, in order to simulate this effect, the secondary reaction K_4 is turned off for the modeled solution. Figure 9 reveals that the model is able to predict the oak pyrolysis products relatively well for both their temporal dependence and final magnitude. The experiments show a small drop in tar yield for the last measurement which may be due to secondary reactions, Neglecting this data point indicates that the final predictions for char, tar and gas are all characterized by $< 4\%$ error. These results suggest that the model is viable as a predictive tool for both tar and gas yields, in addition to residual mass (char). However, tar and gas yield predictions are difficult to compare directly to all but a few existing experiments and further issues associated with such predictions will be delayed for future work.

Ward and Braslaw (1985) studied the pyrolysis of a variety of biomass feedstock under vacuum conditions. The current model is based on results from atmospheric pressure experiments, and hence cannot be expected to agree precisely with the vacuum results. This effect is illustrated in Fig. 10 which depicts the temporal evolution of the residual mass from the pyrolysis of wild cherry wood for both vacuum and atmospheric conditions (Ward and Braslaw, 1985). No scatter was provided in the original citation, and the data in the figure corresponds to points extracted from curve fits. The figure clearly shows a strong influence of pressure on the sample mass, particularly during the early evolution. Although the final residual masses are nearly identical for the two pressures, this type of behavior is not generally observed (see e.g. Güell *et al.*, 1992 for discussions of pressure effects). Agreement between the atmospheric pressure experiments and the present model is excellent. However, the range of pressures for which the present model is capable of making quantitative yield predictions requires further investigation.

A further assessment of the model's capabilities is made through comparison with the low heating rate TGA experiments for bagasse pyrolysis by Varhegyi *et. al.* (1989) (Fig. 11). The heating rate is $10K/\text{min}$, and only the normalized mass rate of change is reported (no yield magnitudes). In addition, only the sample mass (but no apparent density) is reported for this experiment and is listed as $1 - 2\text{mg}$. Estimating an apparent density of $650\text{kg}/\text{m}^3$ (Koufopoulos *et. al.*, 1991), this mass corresponds to a spherical particle with diameter $> 1.5\text{mm}$ and therefore some diffusion effects may be present. Nevertheless, a relatively good qualitative agreement is observed with the kinetic model predictions. Again, there is a delay in the predicted initialization; however, only relatively small mass changes are observed in this region. Although the model does not predict the small initial peak in the data (at $\approx 512\text{K}$), the dominant "double hump" feature observed by the experiments is captured, albeit with peaks occurring at slightly lower temperature. A correction for any possible diffusion effects would move the predicted peaks to larger temperatures and reduce the observed deviations. Varhegyi *et. al.* (1989) were able to fit the untreated bagasse results with a 1.1 % relative error using an assumed independent parallel reaction scheme employing three successive reactions (needed to reproduce the three observed peaks). However, their scheme is based on reaction rates for the conversion variable, $(1 - m)/(1 - m_{\text{char},f})$, which is normalized by the final char yield. Thus, the necessary *a priori* knowledge of the final residual mass removes any predictive capability of the scheme.

A final assessment of the kinetics scheme is performed by evaluating the experimental results of Güell *et. al.* (1992). In this experiment, very small samples of pine wood are heated rapidly (10001/s) from room temperature to final reactor temperatures in the range $573\text{K} \leq T_R \leq 973\text{K}$. The temperature is then held constant for 10s after which the tar and gas collection is ceased and the sample is rapidly quenched. Final residual masses of the samples are reported in Fig. 12 as a function of the holding temperature. The continuous curve in the figure represents the results of 25 simulations with the present kinetic code for evenly spaced final temperatures and duplicated heating conditions. Although the cited work primarily addresses the issue of reactor pressure and its influence, the results contained in the figure are for atmospheric conditions. The nature of this experiment provides a very stringent test of the model's predictive abilities. An excellent qualitative agreement is observed, but with a near constant over-prediction in magnitude. However, the experimental residual particle mass was not measured directly, but was back-calculated from dried tar and vapor masses collected during the pyrolysis. Güell *et. al.* specifically note that some loss of lighter gas phase species mass was observed. In this case, the residual masses reported in Fig. 12 are under-predictions of the true values and the quantitative model predictions are better than suggested by the data,

To this point the agreement between the model predictions and experiments is quite good; however, there are deviations under certain conditions. In particular, the pyrolysis initialization temperature is slightly over

predicted by the model, Fortunately, only relative small percentages of the total conversion generally occur in this region and the effect on the model's predictive ability is small; particularly for high temperature/heating rate pyrolysis. Effects of pressure are not well understood currently (Güell *et al.*, 1992) and the model has therefore been calibrated only for atmospheric pressures. Additional influences on pyrolysis include the possible effects of mineral matter and moisture content. Evans and Milne (1987), and Varhegyi and Antal (1989) showed that such catalysts can have a significant effect on both the pyrolysis evolution and on final char and product yields. In its present form, the current model only treats "typical" (*i.e.* untreated) biomass samples. Further adjustments necessary to include these effects are postponed until a sufficient understanding of pressure effects and catalytic mineral and/or moisture content are available. However, even under its current restrictions, the model provides a robust and viable predictive kinetics scheme for a variety of experimental conditions and applications involving micro-particle biomass pyrolysis.

4 MACRO-PARTICLE MODEL

The new kinetics model assessment of Section 3.2 shows that it compares favorably with both TGA and isothermal pyrolysis experiments for cellulose, lignin, maple, beech wood, oak, wild cherry, bagasse and pine. However, the model is useful for macro-particle pyrolysis predictions only when the kinetics are coupled with a viable particle model with appropriate properties.

4.1 Particle Model

The porous particle model of Miller and Bellan (1996) is used here to model macro-particle pyrolysis for reasons discussed in the introduction and also in the cited work. In summary, the model incorporates all property variations, is valid both inside and outside the particle, and employs a fully transient momentum equation in contrast to the traditional use of the empirical Darcy's Law. The derivation of the model has been addressed previously in Miller and Bellan (1996) and only the final general form of the equations (in spherically symmetric coordinates) is presented here:

$$\frac{\partial \rho_{s,i}}{\partial t} = \dot{S}_{s,i}, \quad (2)$$

$$\frac{\partial \rho_g}{\partial t} + \frac{1}{r^2} \frac{\partial}{\partial r} (r^2 \rho_g u) = \dot{S}_g, \quad (3)$$

$$\frac{\partial \rho_g Y_i}{\partial t} + \frac{1}{r^2} \frac{\partial}{\partial r} (r^2 \rho_g Y_i u - r^2 \rho_g D_{eff}^{(i)} \frac{\partial Y_i}{\partial r}) = \dot{S}_{g,i}, \quad (4)$$

$$\frac{\partial \rho_g u}{\partial t} + \epsilon \left[\frac{\partial}{\partial r} (\rho_g u^2) \right] = -\frac{\partial p}{\partial r} + \frac{1}{r^2} \frac{\partial}{\partial r} \left[r^2 \mu_{eff} \left(2 \frac{\partial u}{\partial r} - \frac{2}{3} \Pi \right) \right] + \frac{4}{3} \frac{\mu_{eff} \Pi}{r} - \frac{4 \mu_{eff} u}{r^2}, \quad (5)$$

$$\frac{\partial e_t}{\partial t} + \frac{1}{r^2} \frac{\partial}{\partial r} \left[r^2 e_g u - r^2 \lambda_{eff} \frac{\partial T}{\partial r} \right] = p \Pi + \sum \dot{S}_i \Delta h_i, \quad (6)$$

$$p = \frac{\rho_g}{\epsilon} \left(\sum Y_i / M_i \right) \bar{RT}, \quad (7)$$

where

$$\rho_g = \varepsilon \hat{\rho}_g, \quad \rho_{s,i} = (1 - \varepsilon) \hat{\rho}_{s,i}, \quad \varepsilon = 1 - \sum^s \rho_{s,i} / \hat{\rho}_{s,i}, \quad (8)$$

$$D_{eff}^{(i)} = \varepsilon D^{(i)}, \quad \mu_{eff} = \varepsilon \sum^g Y_i \mu^{(i)}, \quad (9)$$

$$\lambda_{eff} = (1 - \varepsilon) \left\{ \frac{\sum^s \rho_i \lambda^{(i)}}{\sum^s \rho_i} + \frac{\sigma d T^3}{\omega} \right\} + \varepsilon \sum^g Y_i \lambda^{(i)}, \quad (10)$$

and

$$e_g = \rho_g \left(\sum^g C_v^{(i)} \right) T, \quad e_t = e_g + \left(\sum^s \rho_{s,i} C^{(i)} \right) T. \quad (11)$$

The forms for the reaction source terms (\dot{S}) are derived directly from the kinetics scheme (Fig.4) and the corresponding parameters given in Table 3. In addition to the continuity, momentum, energy and state equations, the full set of governing equations also involves seven solid reactions (virgin plus active for cellulose, hemicellulose and lignin, plus one char) of the form of Eq.(2) and three gas phase mass fraction equations (gas, tar and an inert carrier gas). Note that there are two primary numerical complexities added to the problem by the consideration of the individual biomass components. The first is the addition of several solid reaction equations, and the second is the relatively simple evaluation of additional source terms. However, the solution of the solid reaction equations is straightforward and the computational time is not increased dramatically over the previously published single biomass kinetics (Miller and Bellan, 1996).

4.2 Properties

The macro-particle model is completely determined with the choice of appropriate properties and heats of reaction. Unfortunately, complete information is not always available in the literature. In particular, as mentioned above, there is no data available concerning the properties and/or composition of “active” solid species. Also, while there have been measurements of properties and apparent densities for cellulose and generic wood (e.g. SERI, 1979; Pyle and Zaror, 1984; Curtis and Miller, 1988; Koufopoulos *et. al.*, 1991; Magnaterra *et. al.*, 1992), no similar measurements exist (to our knowledge) for hemicellulose and lignin. In order to make the analysis consistent with available experiment measurements, several assumptions are made concerning the solid phase species. First, it is assumed that the properties and densities of the virgin cellulose, hemicellulose and lignin are the same. Second, the “active” substances are the same as the virgin matrix. Third, the chars produced from the cellulose, hemicellulose and lignin are identical. Fourth, it is assumed that one set of properties can be used to simulate all feedstocks. This assumption is necessary due to the limited number of measurements available and also contributes to the model’s robustness. There are obvious limitations to such an assumption; however, only *a posteriori* analysis of results can determine its extent of validity. Finally, we neglect temperature dependencies of all properties. Properties and information sources for the solid phase species are provided in Table 4, The true

density is calculated based on measurements of both the apparent density and the porosity for both wood and char. Properties for the gas phase species are listed in Table 5; including nitrogen properties which are needed for the inert co-flow. Again, the gas and tar produced from each of the virgin species are assumed identical. The reasons for choosing these sets of solid and vapor properties are discussed below.

Heats of reaction are also needed for every step in the kinetics. There are a variety of measurements and compilations available in the literature from which to choose (Pyle and Zaror, 1984; Curtis and Miller, 1988; Koufopoulos *et al.*, 1991; Di Blasi, 1993a; DiBlasi, 1994). Although some of these measurements have been made for isolated cellulose, similar data is not available for hemicellulose and lignin. It is therefore assumed that each of the four reactions ($K_i, i=1,2,3,4$) is characterized by a single heat of reaction which is independent of the virgin material. Final parameter choices are listed in Table 6 which includes data necessary for the radiation component of the effective thermal conductivity. The initialization reaction K_1 has negligible heat release. The char formation reaction is assumed *exothermic* in agreement with observations: this contrasts with the previous cellulose and wood models compiled by DiBlasi (1992); Di Blasi (1993a); Di Blasi (1993b); Di Blasi (1996). The secondary tar reaction is also exothermic. These parameters completely specify the macro-particle model.

4.-? Model Assessment

In order to assess the viability of the model, an appropriate choice of initial and boundary conditions must be made. The configuration considered is that of a single isolated biomass particle in an initially quiescent environment of super-heated nitrogen. The outer boundary of the computational domain is chosen to be at $R_R = 6R_{p,0}$ for all simulations (see Miller and Bellan, 1996). The choice of nitrogen is dictated by the particular macro-particle experiments used for the model assessment which all employ a co-flowing nitrogen stream (Table 1). The predominant effect of the co-flow on the thermal evolution of a particle is to reduce the thickness of the thermal boundary layer adjacent to the particle, thus moving the "free stream" nearer to the surface. For the pyrolysis considered here, this results in an increase of the effective heating rate. This can be simulated by the current spherically symmetric particle simulations by adjusting the "thermal radius" R_T as described by Miller and Bellan (1996) (R_T is defined such that the temperature is held constant at $T = T_R$ for all positions $r \geq R_T$). Two configurations are chosen: For particles with initial diameters < 1 cm, the thermal radius is $R_T = 2R_{p,0}$ and 48 numerical grid points are found to provide sufficient spatial resolution. For larger particles ($2R_{p,0} \geq 1$ cm), 96 grid points are required and the thermal radius is chosen to be $R_T = 0.1 R_{p,0}$. The values for the thermal radii were chosen rather arbitrarily in order to be consistent with approximate boundary layer thicknesses for flow over spheres (not in order to fit experimental data). The results of Miller and Bellan (1996) show that char yields are not very sensitive to the choice of thermal radius; it is only the conversion time which decreases with decreasing $R_T/R_{p,0}$ for $R_T/R_{p,0} < 3$. The entire domain $r \leq R_R$ is resolved in the simulations in order to

keep track of secondary tar reactions and their effects on the pyrolysis evolution. Boundary conditions and the numerical method are described in detail in Miller and Bellan (1996) and initial conditions are prescribed based on the particular experiment under consideration. All simulations are terminated when the particle mass achieves 99.9% conversion.

The current work employs spherically symmetric particle simulations with only modeled co-flow effects, whereas the experiments used to assess the model are performed in complex reactors and generally employ non-spherical particles (cylindrical, sawdust, wood chip, etc.). Therefore, comparisons with experiments cannot be expected to yield exact quantitative agreements. An additional model specific to each reactor would be needed to insure precise comparisons. Within a reactor model, the present particle model would only be used as a sub-model, coupled through appropriate boundary conditions. This type of approach will be the subject of future investigations.

The first assessment of the macro-particle model is made through a comparison with the isothermal pyrolysis experiments of Maschio *et al.* (1992) where a particle initially at room temperature is exposed to a gaseous nitrogen environment at a uniform temperature $T_R = 773K$. The simulated particle diameter is chosen to match that in the experiments, albeit for cylindrical particles, Geometry and thermal diffusion effects suggest that the spherical symmetry assumption will lead to over-predictions of the cylindrical particle char, particularly for large particle sizes (the area available for heat transfer decreases $\sim r^2$ in spherical coordinates as opposed to $\sim r$ for large aspect ratio cylinders). Figure 13 shows that this is indeed the case. Nevertheless, both the observed trends and the final char yields are well captured by the model. Note that at this temperature, even the smallest particle considered ($R_{p,0} = 250\mu m$) shows deviations from the kinetic limit which are due to finite heating times in addition to exothermic/endothermic reactions. The results of this experiment were used to finalize the choices for the heats of reaction and the apparent density of wood via best visual fit comparisons. However, only options available in the literature were considered with no arbitrary adjustments. Primary heats of reaction (K_2 and K_3) were selected from three available schemes (Pyle and Zaror, 1984; Koufopoulos, 1991; Di Blasi, 1993a) and the apparent density measured by Pyle and Zaror (1984) was also considered in addition to the adopted value. Combinations of parameters other than those employed in Fig. 13 primarily alter the reaction time with only relatively minor effects on the final yields.

The completed macro-particle model can be used to address the issue of the olive husk and poplar wood results previously discussed in relation to Fig. 1. These experiments were performed in a semi-batch bench scale reactor by Maschio *et al.* (1992). Although the authors report particle sizes for both TGA ($< 0.5mm$) and isothermal ($0.3 - 20mm$) experiments, no particle size is reported for the batch pyrolysis. In order to explain the results for the poplar and olive husk, numerical simulations are conducted for conditions similar to the isothermal cases

described above. The finite particle size is chosen arbitrarily to be $R_{p,0} = 2.5\text{mm}$ for both feedstocks [Miller and Bellan (1996) show that the char yield increases with increasing particle size due to lower effective pyrolysis temperatures]. Figure 14 presents the experimental data in comparison with the numerical predictions and also the kinetic limits from the micro-particle model. Although the model's accuracy may not be sufficient to predict the exact size of the particles used in the experiment, the results suggest that there are macro-particle effects present. Clearly, only at the lowest reactor temperatures can these particles be well described by kinetic modeling (Simmons and Gentry, 1986). Improvements in the agreement for the olive husk pyrolysis could be made by decreasing the assumed particle size; however, this is not necessary at the current time and it was considered more important to maintain a consistent particle size for both feedstocks.

The results of Fig. 14(b) for olive husk pyrolysis reveal an interesting behavior at the lowest reactor temperature ($T_R = 623\text{K}$). In this case, both the model prediction and the experimental data fall *below* the kinetically controlled pyrolysis limit. This indicates that the majority of pyrolysis is actually occurring for temperatures larger than the reactor temperature and is confirmed by Maschio *et al.* (1992). Figure 15 illustrates this effect through the temporal evolution of the mass averaged particle temperature from the macro-particle model for each of the simulated reactor temperatures. The mass averaging is over solid phase species but does not include the char;

$$\langle T' \rangle = \frac{\int_0^\infty 4\pi r^2 \rho'_s T' \cdot dr}{\int_0^\infty 4\pi r^2 \rho'_s \cdot dr} \quad (12)$$

(see also Miller and Bellan, 1996), and time is normalized by the conversion time (99.9% conversion). For large reactor temperatures, $\langle T' \rangle$ increases monotonically and the pyrolysis occurs at temperatures less than the reactor conditions. However, for $T_R = 623\text{K}$ an overshoot is observed in the particle temperature at early times. The overshoot is caused by the relatively large char production at low temperatures. The exothermic char forming reaction (K_3) dominates under these conditions and thermal overshoots result. Note that the three distinct pyrolysis regimes identified by Miller and Bellan (1996) are not observed in Fig. 15. This is due to the relatively large temperature range over which the pyrolysis occurs for the present reaction scheme and due to the three superimposed thermal reaction rate peaks (see Fig. 7). Single component pyrolysis (e.g. CCIU1OSC) displays a single sharp thermal peak in reaction rate and more clearly exhibits the pyrolysis regimes (Miller and Bellan, 1996; Narayan and Antal, 1996). Thermal overshoots are corroborated by past low temperature pyrolysis experiments by Koufopoulos *et al.* (1991) and Maschio *et al.* (1992). In addition, Mok *et al.* (1992) correlated the apparent heat of reaction from pyrolysis with the char yield and observed that large char yields (low temperatures) are associated with net exothermic reactions. The single and successive step reactions postulated by Mok *et al.* (1992) cannot be reconciled with this behavior, unless the heat of reaction is forced to be a function of temperature, contrary to its thermodynamic definition. In contrast, the present model, which uses

a competitive reaction scheme with constant heats of reaction and constant Arrhenius parameters (in agreement with thermodynamic and kinetic definitions), both predicts and explains these observations.

The final two sets of experimental results simulated with the present model are both for the pyrolysis of large ($> 2\text{cm}$) pine wood samples. Pyle and Zaror (1984) report the temporal evolution of the conversion variable for cylindrical pine samples (diameter equal to 2.2cm) under isothermal pyrolysis conditions at both $T_R = 643\text{K}$ and $T_R = 753\text{K}$. The macro-particle model is used to simulate these conditions using the method described above and room temperature initial conditions for the particle. Comparisons are made in Fig. 16. Although the model predictions lag the experimental data, the overall agreement is reasonable. It is not possible at this point to distinguish the influence of the sample geometry on the results; however, as described above, corrections for these effects would improve the predictions. Final char yields are not reported in the cited work, hence such comparisons are not possible.

Bilbao *et al.* (1992) also investigate pine wood pyrolysis. They consider the TGA pyrolysis of spherical samples at relatively low heating rates. In general, the numerical time step requirements prohibit the simulation of TGA experiments for small particle sizes. However, the large particles used in the Bilbao *et al.* experiments relax the time step restrictions and allow simulations to be performed with acceptable computer processor times ($< 1200\text{s}$ on a Cray YMP). The spherical samples employed in their work are also consistent with the current spherically symmetric particle model. Nevertheless, the experimental findings show that results are substantially dependent on the measurement angle with respect to the co-flow which may influence the accuracy of the comparisons.

Figure 17 compares the experimental results for a TGA case with a heating rate of $12\text{K}/\text{min}$ for various particle sizes (up to $2R_{p,0} = 5.6\text{cm}$). To simulate the TGA experiment with the current model, the entire numerical domain is initially at 303K and the reactor temperature (outer boundary condition) is raised linearly in time to match the experimental conditions. The comparisons reveal several trends already discussed for the micro-particle model TGA simulations. That is, there is a significant delay in the initialization of the pyrolysis process associated with the low temperature behavior of the kinetic parameters. Although the simulations predict a nearly identical final yield independent of initial particle size, the expected behavior is not clear from the experiments. The two larger experimental particle sizes appear to show nearly the same final char yield; however, there is large scatter in the data from the $R_{p,0} = 2.8\text{cm}$ particle and definite conclusions cannot be made. Other experiments reported by Bilbao *et al.* (1992) at lower heating rates show a stronger convergence of final yields (not shown). Nevertheless, the yield predicted by the model is larger than that observed in any of the experiments. At best, the macro-particle model is able to give a qualitative description of the pyrolysis evolution and to provide a fairly acceptable prediction of the pyrolysis yields. The comparisons improve if corrections are made for the delay in

pyrolysis initialization. We note here that the agreement improves with decreasing particle sizes, and that the particles considered by Bilbao *et al.* are much larger than those used in the majority of pyrolysis applications.

It is useful to compare predictions from the current model with those of the macro-particle wood model investigated by Miller and Bellan (1996). It was already noted when discussing Fig. 15 that the three pyrolysis regimes observed by Miller and Bellan (1996) are no longer distinct in the new model. In particular, the near constant “effective pyrolysis temperature” which characterized the second regime no longer exists because of the overlapping pyrolysis thermal regions due to the superposition of cellulose, hemicellulose and lignin. The question occurs as to how this might change predictions and optimization of tar production in commercial reactors. Miller and Bellan (1996) explained optimal temperatures for tar maximization observed in the experiments of Scott and Piskorz (1982); Scott *et al.* (1988); Lidén *et al.* (1988) in terms of competing rates of tar production from the biomass and tar decomposition reactions to gas. These latter reactions dominate at large temperatures thus reducing the actual mass of tar which can be harvested from the mass boundary layer exterior to the particle.

Figure 18 illustrates this effect for both the current model (oak) and the wood model previously studied by Miller and Bellan (1996). The “5% tar radius” is the maximum normalized radius at which the tar mass fraction has decayed to 0.05 and the maximum tar mass fraction is over the entire domain (‘maximum’ includes all times). The “5% tar radius” provides a measure of how closely to the particle the tar is distributed whereas the mass fraction is indicative of the total tar produced. All initial and boundary conditions are kept constant for both particles; $R_{p,0} = 0.005m$, $R_R = 10R_{p,0}$, $R_T = 5R_{p,0}$, $T_{p,0} = 300K$ and remaining parameters as given previously. Both models display a monotonically decreasing 5% tar radius indicating that larger reactor temperatures result in higher tar conversion rates (to gas) and hence tar distributions closer to the particle surface. An opposite trend is observed in the maximum tar fraction. As discussed in Miller and Bellan (1996) the Model 1 wood results show a monotonically increasing maximum tar fraction indicating increasing tar production with reactor temperature. However, the current model shows the opposite behavior for the maximum tar fraction; *i.e.* monotonically decreasing. Further, both the 5% radius and the tar fractions are always larger for the current model than for Model 1. The reasons for these behaviors are directly related to the three superimposed kinetics and the lack of an effective pyrolysis temperature. First, the new model clearly produces more tar than does Model 1 of Miller and Bellan (1996); hence both parameters are larger for the current model in Fig. 18. Second, the lack of the near constant effective pyrolysis temperature results in larger particle (reaction) temperatures for the new model [as seen from comparing the current Fig. 15 with Fig. 9 of Miller and Bellan (1996)]. In fact, the tar production actually increases with reactor temperature; however, higher particle temperatures result in relatively large tar decomposition rates which overcome the increased production rates and decrease the maximum tar fraction. Nevertheless, optimal reactor temperatures for tar production remain possible: The challenge is to avoid

tar decomposition to gas as far as possible from the particle surface. These issues will be further addressed in a forthcoming paper.

5 CONCLUSIONS AND DISCUSSIONS

A mathematical model is presented for modeling both micro-particle (kinetically controlled) and macro-particle (diffusion limited) pyrolysis of arbitrary biomass feedstocks. The micro-particle model is based on a superposition of kinetics of the primary components of biomass; CELLULOSE, hemicellulose and lignin. All three reaction schemes are based on the model of Bradbury *et. al.* (1979) as adjusted by DiBlasi (1994) to include secondary tar decomposition." Char formation is via competitive primary reactions of the active feedstock. The kinetic parameters for cellulose are taken to be identical to those used by DiBlasi (1994) while the hemicellulose and lignin parameters are modified from previous schemes to fit the results of three experiments for beech wood, lignin and maple wood pyrolysis. The model is intended for "typical" feedstock specimens and atmospheric pyrolysis pressures; modifications necessary for pressure, mineral and/or moisture content are delayed for future work. Nevertheless, further comparisons with experiments *not* used to fit the kinetic parameters show good agreement with previous micro-particle experiments of bagasse, cellulose, cherry wood, oak and pine for a large variety of both TGA and isothermal pyrolysis conditions. Considering the large variation of the three primary components of biomass in these feeds (0.22 – 0.50 for cellulose; 0.27- 0.47 for hemicellulose; 0.17- 0.45 for lignin), the kinetics model displays an unprecedented robustness.

Discussions are also included which address the issue of secondary char production mechanism models (as opposed to primary), which interpret char production as occurring through secondary catalytic reactions of vapor pyrolysis products with the solid matrix. However, secondary char production models currently lack a credible kinetics and they are limited to single step and/or successive reaction schemes (e.g. Varhegyi *et. al.*, 1989) which predict constant char yields independent of the pyrolysis temperature (due to their non-competitive charring). The current discussions show clearly that these models cannot be reconciled with known pyrolysis behavior, and therefore do not have predictive value.

The kinetic schemes developed for the biomass components are then incorporated into the previous porous particle model of Miller and Bellan (1996) in order to model macro-particle pyrolysis. Appropriate choices of properties and heats of reaction complete the model. The predicted results are compared to previous experiments of beech wood, olive husk, pine and poplar wood under a variety of conditions. Comparisons show good qualitative agreement in all cases with quantitative agreements improving for decreasing particle sizes and increasing reactor temperatures. In general, final char yields are well predicted while the pyrolysis duration may be over predicted for particles larger than ≈ 1 cm. It is also shown that the experimental results for both poplar and olive husk can

be explained in terms of macro-particle effects (although no sizes were originally reported). In addition, the model predicts thermal overshoots for low temperatures (due to exothermic char formation) which are in agreement with the observations of several experiments and are well explained in terms of the competitive charring mechanism.

Although the macro-particle model is capable of making robust predictions of pyrolysis behavior for a variety of conditions and feedstocks, there remains room for improving its accuracy. There are a variety of possible explanations for the deviations observed in the macro-particle pyrolysis comparisons. Favorable results for the micro-particle comparisons suggest that the deviations are not primarily due to flaws in the kinetics. One possible source of discrepancies may be introduced by the mineral matter present in the wood used in the experiments acting as a catalyst; the current model does not address this issue. Geometry differences between the macro-particles used in the experiments and the spherical symmetry assumption used in the macro-particle calculations certainly affect the comparisons. Large aspect ratio cylindrical particles may be modeled using a one dimensional domain in cylindrical coordinates; however, more moderate aspect ratios will require multi-dimensional axisymmetric coordinate simulations for accurate model assessments. It is also difficult to assess the influence of asymmetry due to the nitrogen co-flow used in experiments, and/or the use of the thermal radius to model these effects. Other obvious influences are connected with the properties used in the particle model. Deviations with experimental results could be due to differences between various feedstock properties and those in the model; for example, the largest observed deviations are both for pine wood samples which may have substantially different properties than the assumed values. The predominant properties affecting the pyrolysis are those which directly affect the thermal evolution, *i.e.* thermal conductivity, heat capacity and initial apparent density. At this point, it is not possible to distinguish the extent of contribution from each of the above factors and future research in these areas is necessary.

ACKNOWLEDGMENTS

This research was conducted at the Jet Propulsion Laboratory (JPL) and sponsored by the U.S. Department of Energy (DOE), with Mr. Neil Rossmeissl (DOE Headquarters) and Mr. D. Hooker (DOE Golden Center) serving as contract monitors, under an agreement with the National Aeronautics and Space Administration. Computational resources are provided by the super computing facility at JPL. The authors wish to thank Dr. Esteban Chornet for suggesting the superposition of cellulose, hemicellulose and lignin kinetics to represent biomass kinetics, and Dr. Robert Evans of the National Renewable Energy Laboratory for helpful discussions.

REFERENCES

- Antal, M. J. Biomass pyrolysis: A review of the literature. part 1. Carbohydrate pyrolysis. In K. Boer and J. Duffie, editors, *Advances in Solar Energy*, pages 61-111. American Solar Energy Society, Boulder, CO, 1982.
- Antal, M. J. and Mok, W. S. L. Review of methods for improving the yield of charcoal from biomass. *Energy and Fuels*, 4(3):221-225, 1990.
- Antal, M. J. and Varhegyi, G. Cellulose pyrolysis kinetics: The current state of knowledge. *Ind. Eng. Chem. Res.*, 34(3) :703-717, 1995.
- Bilbao, R., Millera, A., and Murillo, M. B. Heat transfer and weight loss in the thermal decomposition of large wood particles. in A. V. Bridgwater, editor, *Advances in thermochemical Biomass Conversion*, volume 2, pages 833-845. Blackie Academic and Professional, New York, New York, 1992.
- Bradbury, A. G., Sakai, Y., and Shafizadeh, F. A kinetic model for pyrolysis of cellulose. *J. App. Polymer Sci.*, 23:3271-3280, 1979.
- Chan, W. R., Kelbon, M., and Krieger-Brockett, B. Modeling and experimental verification of physical processes during pyrolysis of a large biomass particle. *Fuel*, 64:1505-1513, 1985.
- CRC. *CRC Handbook of Chemistry and Physics*. CRC Press, Inc., Ann Arbor, MI, 1992.
- Curtis, L. J. and Miller, D. J. Transport model with radiative heat transfer for rapid cellulose pyrolysis. *Ind. Eng. Chem. Res.*, 27:1775-1783, 1988.
- Di Blasi, C. Modeling of transport phenomena and kinetics of biomass pyrolysis. in A. V. Bridgwater, editor, *Advances in Thermochemical Biomass Conversion*, volume 2, pages 906-921. Blackie Academic and Professional, New York, New York, 1992.
- Di Blasi, C. Analysis of convection and secondary reaction effects within porous solid fuels undergoing pyrolysis. *Combust. Sci. and Tech.*, 90:315-340, 1993a.
- Di Blasi, C. Modeling and simulation of combustion processes of charring and non-charring solid fuels. *Prog. Energy Combust. Sci.*, 19:71-104, 1993b.
- Di Blasi, C. Numerical simulation of cellulose pyrolysis. *Biomass and Bioenergy*, 7:87-98, 1994.
- Di Blasi, C. Kinetic and heat transfer control in the slow and flash pyrolysis of solids. *Ind. Eng. Chem Res.*, 35:37-46, 1996.
- Dicbold, J. P. and Power, A. Engineering aspects of the vortex pyrolysis reactor to produce primary pyrolysis oil vapors for use in resins and adhesives. In A. V. Bridgwater and J. L. Kuester, editors, *Research in Thermochemical Biomass Conversion*, pages 609-628, Elsevier Applied Science, New York, New York, 1988,

- Evans, R. J. Personal communication, Apr. 1996.
- Evans, R. J. and Milne, T. A. Molecular characterization of the pyrolysis of biomass, 1. Fundamentals. *Energy and Fuels*, 1(2):123-137, 1987.
- Guell, A. J., Li, C. Z., Herod, A. A., Stokes, B. J., Hancock, P., and Kandiyoti, R. Mild hydrolysis of biomass materials: Effect of pressure on product tar structures. In A. V. Bridgwater, editor, *Advances in Thermochemical Biomass Conversion*, volume 2, pages 1053-1067. Blackie Academic and Professional, New York, New York, 1992.
- Hallgren, A. and Wanzl, W. Screening of pyrolysis behavior of different biomass, In A. V. Bridgwater, editor, *Advances in Thermochemical Biomass Conversion*, volume 2, pages 806-817. Blackie Academic and Professional, New York, New York, 1992.
- Kansa, E. J., Perleo, H. E., and Chalken, R. F. Mathematical model of wood pyrolysis including internal forced convection. *Comb. and Flame*, 29:311-324, 1977.
- Kothari, V. and Antal, M. J. Numerical studies of the flash pyrolysis of cellulose. *Fuel*, 64:1487-1494, 1985.
- Koufopoulos, C. A., Maschio, G., and Lucchesi, A. Kinetic modelling of the pyrolysis of biomass and biomass components. *Can. J. Chem. Eng.*, 67:75-84, 1989.
- Koufopoulos, C. A., Papayannakos, N., Maschio, G., and Lucchesi, A. Modelling of the pyrolysis of biomass particles. Studies on kinetics, thermal and heat transfer effects. *Can. J. Chem. Eng.*, 69:907-915, 1991.
- Lede, J., Panagopoulos, J., Li, H. Z., and Villermaux, J. Fast pyrolysis of wood: Direct measurement and study of ablation rate. *Fuel*, 64:1514-1520, 1985.
- Lewellen, P. S., Peters, W. A., and Howard, J. B. Cellulose pyrolysis kinetics and char formation mechanism. In 16th Symposium (International) on Combustion, pages 1471-1479. 1976.
- Liden, A. G., Berruti, F., and Scott, D. S. A kinetic model for the production of liquids from the flash pyrolysis of biomass. *Chem. Eng. Comm.*, 65:207-221, 1988.
- Madonsky, S. L. *Thermal Degradation of Organic Polymers*. Interscience, New York, New York, 1964.
- Magnaterra, M., Fusco, J. R., Ochoa, J., and Cukierman, A. I. Kinetic study of the reaction of different hardwood sawdust chars with oxygen. Chemical and structural characterization of the samples. In A. V. Bridgwater, editor, *Advances in Thermochemical Biomass Conversion*, volume 1, pages 116-130, Blackie Academic and Professional, New York, New York, 1992.
- Maschio, G., Lucchesi, A., and Koufopoulos, C. A. Study of kinetic and transfer phenomena in the pyrolysis of biomass particles. In A. V. Bridgwater, editor, *Advances in Thermochemical Biomass Conversion*, volume 2, pages 746-759. Blackie Academic and Professional, New York, New York, 1992.
- Miller, R. S. and Bellan, J. Analysis of reaction products and conversion time in the pyrolysis of cellulose

and wood particles. *Comb. Sci.Tech.*, 1996. In Press.

Mok, W. S., Antal, M. J., Szabo, P., Varhegyi, G., and Zeleci, B. Formation of charcoal from biomass in a scaled reactor. *Ind.Eng.Chem. Ms.*, 31:11 62–1166, 1992,

Narayan, R. and Antal, M. J. Thermal lag, fusion, and the compensation effect during biomass pyrolysis, *Ind. Eng. Chem. Res.*, 1996. submitted.

Pyle, D. L. and Zaror, C. A. Heat transfer and kinetics in the low temperature pyrolysis of solids. *Chem. Eng. Sci.*, 39(1):147–158, 1984.

Scott, D. S. and Piskorz, J. The flash pyrolysis of aspen-poplar wood. *Can. J. Chem. Eng.*, 60:666–674, 1982.

Scott, D. S., Piskorz, J., Bergougnou, M. A., Graham, R., and Overend, R. P. The role of temperature in the fast pyrolysis of cellulose and wood. *Ind. Eng. Chem. Res.*, 27:8-15, 1988.

SERI. A survey of biomass gasification: Volume 11- Principles of gasification, Technical Report TR-33-239, Solar Energy Research Institute, Golden, Colorado, July 1979.

Shafizadeh, F., Furneaux, R. H., Cochran, T. G., Scholl, J. P., and Sakai, Y. Production of levoglucosan and glucose from pyrolysis of cellulosic materials. *J. Appl. Polym. Sci.*, 23:3525–3539, 1979.

Simmons, G. M. and Gentry, M. Particle size limitations due to heat transfer in determining pyrolysis kinetics of biomass. *J. Anal. and Appl. Pyrolysis*, 10:117-127, 1986.

Turner, F. and Marm, U. Kinetic investigation of wood pyrolysis. *Ind. Eng. Chem. Process Des. Dev.*, 20:482–488, 1981.

Varhegyi, G., Antal, M. J., Szekely, T., and Szabo, P. Kinetics of the thermal decomposition of cellulose, hemicellulose, and sugar cane bagasse. *Energy and Fuels*, 3:329-335, 1989.

Varhegyi, G., Jakab, E., and Antal, M. J. Is the Broido-Shafizadeh model for cellulose pyrolysis true? *Energy and Fuels*, 8: 1345–1352, 1994.

Ward, S. M. and Braslaw, J. Experimental weight loss kinetics of wood pyrolysis under vacuum. *Comb. and Flame*, 61:261-269, 1985.

TABLES

| Biomass | Type | Size [mm] | $\frac{dT_R}{dt}$ [$\frac{K}{min}$] | T_R [K] | Class | Source |
|------------|------|------------------|---------------------------------------|----------------------------|-------|-----------------------------------|
| Beech* | TGA | 0.3--0.85 | 5 - 80 | | I | Koufopoulos <i>et. al.</i> (1989) |
| Lignin* | 1s0 | < 1.0 | | 673,873 | I | Koufopoulos <i>et. al.</i> (1989) |
| Maple* | 1s0 | 0.120 | | 673--1073 | I | Scott <i>et. al.</i> (1988) |
| Cellulose | 1s0 | < 1.0 | | 600- 775 | I | Shafizadeh <i>et. al.</i> (1979) |
| Cellulose | 1s0 | 0.1 | | 723 - 873 | I | Scott <i>et. al.</i> (1988) |
| Bagasse | TGA | $\sim 1^\dagger$ | 10 | - | I | Varhegyi & Antal (1989) |
| Cherry | 1s0 | 0.25 | - | 573 | I | Ward & Braslaw (1985) |
| Oak | 1s0 | 0.840 | \ddagger | 642 | I | Turner & Mann (1981) |
| Pine | 1s0 | 0.10--0.15 | 1000 | 573-- 973 $\dagger\dagger$ | I | Güell <i>et. al.</i> (1992) |
| Beech | 1s0 | 0.5- 20 | | 773 | II | Maschio <i>et. al.</i> (1992) |
| Olive husk | ISO | $\sim 1^\dagger$ | - | 623--823 | II | Maschio <i>et. al.</i> (1992) |
| Pine | TGA | 20- 56 | 12 | 923 | II | Bilbao <i>et. al.</i> (1992) |
| Pine | 1s0 | 22 | - | 643,753 | II | Pyle & Zaror (1984) |
| Poplar | 1s0 | $\sim 1^\dagger$ | | 623- 823 | II | Maschio <i>et. al.</i> (1992) |

Table 1: Description of biomass pyrolysis experiments used for comparisons. The listed information includes the experiment type (TGA = thermogravimetry, 1 SO = isothermal), sample size, heating rate, reactor temperatures and the classification (I = kinetic control, II = macro particles). The * indicates results used to develop the current model; \dagger indicates an estimate, since there was no reported value; \ddagger refers to a modeled heating rate to the final temperature to fit the reported results (see text); and $\dagger\dagger$ indicates a 10s holding time at the final temperature.

| Biomass | Cellulose | Hemicellulose | Lignin | Source |
|------------|-----------|---------------|--------|-------------------------------|
| Bagasse | 0.36- | 0.47 | 0.17 | Mok <i>et. al.</i> (1992) |
| Beech | 0.48 | 0.28 | 0.24 | Maschio <i>et. al.</i> (1992) |
| Cherry | 0.42 | 0.34 | 0.24 | Ward & Braslaw (1985) |
| Maple | 0.40 | 0.38 | 0.22 | Mok <i>et. al.</i> (1992) |
| Oak | 0.35 | 0.40 | 0.25 | SERI (1979) |
| Olive husk | 0.22 | 0.33 | 0.45 | Maschio <i>et. al.</i> (1992) |
| Pine | 0.50 | 0.27 | 0.23 | Ward & Braslaw (1985) |
| Poplar | 0.48 | 0.30 | 0.22 | Maschio <i>et. al.</i> (1992) |

Table 2: Biomass compositions by mass used in this study. All extractive and ash content are included with the hemicellulose.

| Reaction | A_i [1/s] | E_i [KJ/mol] | Source |
|----------|-----------------------|----------------|-----------------------------|
| K_1^c | 2.8×10^{19} | 242.4 | Di Blasi (1994) |
| K_2^c | 3.28×10^{14} | 196.5 | » |
| K_3^c | 1.3×10^{10} | 150.5 | » |
| K_1^h | 2.1×10^{16} | 186.7 | Ward & Braslaw (1985)* |
| K_2^h | 8.75×10^{15} | 202.4 | Di Blasi (1994)' |
| K_3^h | 2.6×10^{11} | 145.7 | » |
| K_1^l | 9.6×10^8 | 107.6 | Ward & Braslaw (1985)* |
| K_2^l | 1.5×10^9 | 143.8 | Koufopoulos et. al. (1989)' |
| K_3^l | 7.7×10^6 | 111.4 | » |
| K_4 | 4.28×10^6 | 108.0 | Di Blasi (1994) |

Table 3: Reaction parameters. The char formation mass ratios for reaction K_3 are; $X^c = 0.35$, $X^h = 0.60$ and $X^l = 0.75$ and the superscript * indicates modified values.

| Species | Property | Value | Source |
|---------|--------------|---|----------------------------|
| wood | ρ_0 | $650 \frac{kg}{m^3}$ | Koufopoulos et. al. (1991) |
| | ϵ_0 | 0.7 | SERI (1979) |
| | $\hat{\rho}$ | $2167 \frac{kg}{m^3}$ | |
| | C | $2.3 \frac{kJ}{kg \cdot K}$ | Curtis & Miller (1988) |
| char | λ | $1.256 \times 10^{-4} \frac{kJ}{m \cdot s \cdot K}$ | Pyle & Zaror (1984) |
| | ρ | $350 \frac{kg}{m^3}$ | » |
| | ϵ | 0.85 | Magnaterra et. al. (1992) |
| | $\hat{\rho}$ | $2333 \frac{kg}{m^3}$ | |
| | C | $1.1 \frac{kJ}{kg \cdot K}$ | Curtis & Miller (1988) |
| | λ | $8.37 \times 10^{-5} \frac{kJ}{m \cdot s \cdot K}$ | Pyle & Zaror (1984) |

Table 4: Property values for the solid phase species.

| Species | Property | Value | Source |
|----------|-----------|---|-----------------------------|
| gas | M | $30 \frac{\text{kg}}{\text{kg}\cdot\text{mole}}$ | Evans (1996) |
| | C_v | $1.1 \frac{\text{kJ}}{\text{kg}\cdot\text{K}}$ | DiBlasi (1993a) |
| | λ | $2.577 \times 10^{-5} \frac{\text{kJ}}{\text{m}\cdot\text{s}\cdot\text{K}}$ | " |
| | μ | $3.0 \times 10^{-5} \frac{\text{kg}}{\text{m}\cdot\text{s}}$ | Kansa <i>et. al.</i> (1977) |
| | D | $1.1 \times 10^{-4} \frac{\text{m}^2}{\text{s}}$ | Miller & Bellan (1996) |
| tar | M | $100 \frac{\text{kg}}{\text{kg}\cdot\text{mole}}$ | Evans (1996) |
| | C_v | $2.5 \frac{\text{kJ}}{\text{kg}\cdot\text{K}}$ | Curtis & Miller (1988) |
| | λ | $2.577 \times 10^{-5} \frac{\text{kJ}}{\text{m}\cdot\text{s}\cdot\text{K}}$ | Miller & Bellan (1996) |
| | μ | $3.0 \times 10^{-5} \frac{\text{kg}}{\text{m}\cdot\text{s}}$ | Kansa <i>et. al.</i> (1977) |
| | D | $1.1 \times 10^{-4} \frac{\text{m}^2}{\text{s}}$ | Miller & Bellan (1996) |
| nitrogen | M | $28.013 \frac{\text{kg}}{\text{kg}\cdot\text{mole}}$ | (RC (1992)) |
| | C_v | $0.8246 \frac{\text{kJ}}{\text{kg}\cdot\text{K}}$ | " |
| | λ | $5.63 \times 10^{-5} \frac{\text{kJ}}{\text{m}\cdot\text{s}\cdot\text{K}}$ | " |
| | μ | $3.58 \times 10^{-5} \frac{\text{kg}}{\text{m}\cdot\text{s}}$ | " |
| | D | $8.52 \times 10^{-4} \frac{\text{m}^2}{\text{s}}$ | Unit Lewis Number |

Table 5: Property values for the gas phase species. The properties for nitrogen are taken at $T = 800\text{K}$ and $p = 100\text{kPa}$.

| Property | Value | Source |
|--------------|-------------------------------------|-----------------------------------|
| Δh_1 | 0 | DiBlasi (1994) |
| Δh_2 | $-4255 \frac{\text{kJ}}{\text{kg}}$ | Koufopoulos <i>et. al.</i> (1991) |
| Δh_3 | $-20 \frac{\text{kJ}}{\text{kg}}$ | Koufopoulos <i>et. al.</i> (1991) |
| Δh_4 | $-42 \frac{\text{kJ}}{\text{kg}}$ | Curtis & Miller (1988) |
| d | $4 \times 10^{-7} \text{m/s}$ | Chan <i>et. al.</i> (1985) |
| w | 0.95 | Pyle & Zaror (1984) |

Table 6: Miscellaneous values used in the particle model,

FIGURE CAPTIONS

Figure 1: Comparison of final isothermal char yields as a function of the reactor temperature. The symbols represent experimental data; poplar wood (o) and olive husk (Δ) by Maschio *et. al.* (1992), oak (\square) by Thurner and Mann (1981) and maple (.) by Scott *et. al.* (1988). The solid lines represent model predictions for wood pyrolysis; (1) Di Blasi model kinetics with Thurner and Mann's original kinetic parameters, (2) Ward and Braslaw (1985) and (3) Koufopoulos *et. al.* (1989). The dotted line indicates the new model and all feedstock dependent models are applied to maple.

Figure 2: isothermal char yields as a function of temperature for primary biomass components as predicted by the Koufopoulos *et. al.* (1989) kinetics.

Figure 3: Comparison of final char yields from isothermal cellulose pyrolysis as a function of temperature. The symbols represent the experiments of Shafizadeh *et. al.* (1979) (\blacklozenge) and Scott *et. al.* (1988) (\square) and the solid lines represent the kinetic model predictions of Bradbury *et. al.* (1979) (I) and the kinetic model of Koufopoulos *et. al.* (1989) (II).

Figure 4: Generic reaction scheme used to model cellulose, hemicellulose and lignin kinetics.

Figure 5: isothermal normalized mass evolution for lignin. Experimental results of Koufopoulos *et. al.* (1989) (symbols) in comparison with the model predictions (solid lines),

Figure 6: Comparison of the model predictions with TGA experiments for beech wood. The symbols represent data points extracted from the experimental curve fits of Koufopoulos *et. al.* (1989) for heating rates of 5K/min (\circ), 20K/min (\square) and 80K/min (Δ).

Figure 7: Normalized mass reduction rate predicted by the kinetic model for TGA with a 10K/min heating rate for cellulose (c.), hemicellulose (h.) and lignin (l.). The normalization is by the maximum value for cellulose.

Figure 8: isothermal char yields as a function of temperature for primary biomass components as predicted by

the modeled kinetics.

Figure 9: Normalized mass evolutions for isothermal oak pyrolysis at $T_R = 642K$. The symbols represent the experimental measurements of Thurner and Mann (1981) for the residual (.), tar (A) and gas (■) mass. The solid line represent the kinetic model mass predictions with $A_4 = 0$ and the dotted line indicates the modeled reactor temperature evolution, Mass is normalized by the initial sample mass.

Figure 10: Residual mass evolution for isothermal pyrolysis of cherry wood at $T_R = 573K$. The symbols represent data points extracted from the experimental curve fits of Ward and Braslaw (1985) at both vacuum and ambient pressures.

Figure 11: Comparison of the normalized mass evolution for TGA of untreated bagasse at a heating rate of $10K/min$. The solid line is the kinetic model prediction and the symbols are experimental results of Varhegyi and Antal (1989). Normalization is with the maximum value.

Figure 12: Comparison of kinetic model predictions with experimental results of Güell *et. al.* (1992) for final residual mass from pine wood pyrolysis. The experimental condition modeled is a pine wood sample initially at room temperature and then heated at $10001 \text{ } ^\circ\text{C/s}$ to the final holding temperature with a 10s hold.

Figure 13: Comparison of experimental (symbols) residual mass evolutions for isothermal pyrolysis of beech wood at $T_R = 773K$ (Maschio *et. al.*, 1992) with the full particle model (solid lines). The particle diameters are; $0.5mm$ (1, ●), $3mm$ (2, △), $8mm$ (3, ○) and $20mm$ (4, El) and the dotted line (0) indicates the predicted kinetic limit.

Figure 14: Final char yields for isothermal pyrolysis of (a) poplar wood and (b) olive husk. Experimental results are from Maschio *et. al.* (1992) and the full particle model predictions are based on an estimated particle diameter of $5mm$.

Figure 15: Normalized mass averaged particle temperature evolution predicted by the full particle model for the olive husk simulations of Fig. 14(b).

Figure 16: Comparison of conversion evolutions for isothermal pine wood pyrolysis from experiments by Pyle and Zaror (1984) and the full particle model predictions with $R_{p,0} = 1.1 \text{ cm}$. The experimental results are indicated by the symbols and correspond to reactor temperatures; $T_R = 643 \text{ K}$ (\circ) and $T_R = 753 \text{ K}$ (\square).

Figure 17: Comparison of residual mass evolutions for TGA pine wood pyrolysis from experiments by Bilbao *et al.* (1992) and the full particle model for various particle sizes. The heating rate is 12 K/min and the final holding temperature is $T_R = 923 \text{ K}$. The experimental results are indicated by the symbols; $R_{p,0} = 1.0 \text{ cm}$ (\circ), $R_{p,0} = 2.0 \text{ cm}$ (\blacklozenge) and $R_{p,0} = 2.6 \text{ cm}$ (\square).

Figure 18: Maximal normalized radial position at which the tar fraction has decayed to 5% and the maximum tar mass fraction as a function of the reactor temperature for both the wood model from Miller and Bellan (1996) (Model 1) and the current model for oak (Model 11); $R_{p,0} = 0.005 \text{ m}$, $R_R = 10R_{p,0}$, $R_T = 5R_{p,0}$, $T_{p,0} = 300 \text{ K}$.

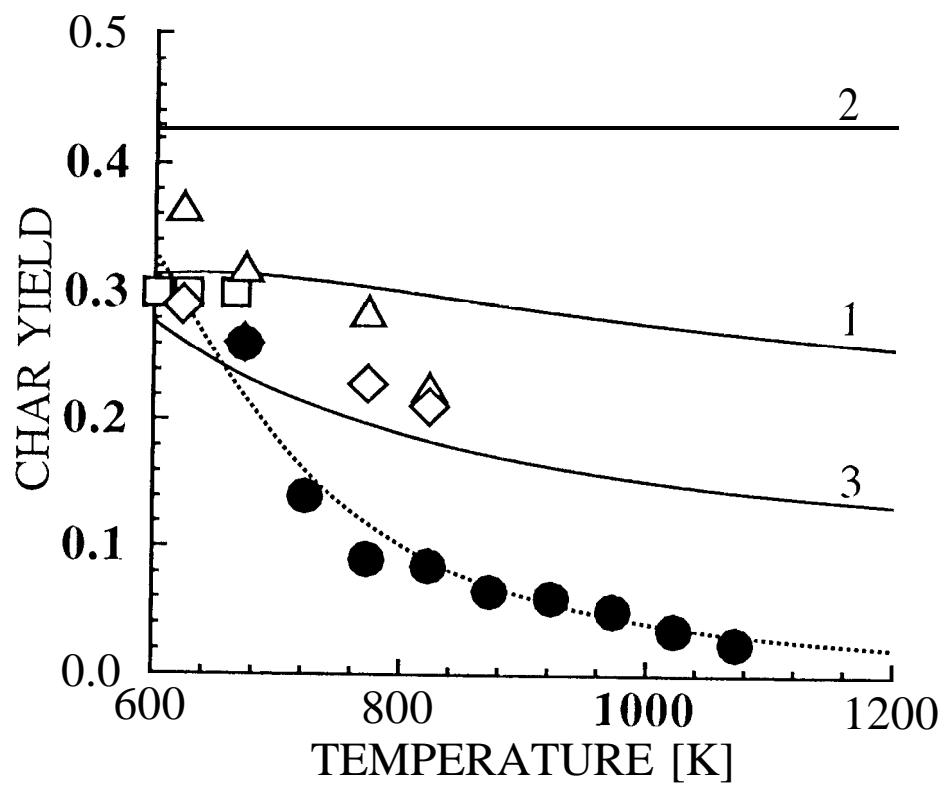


Figure 1

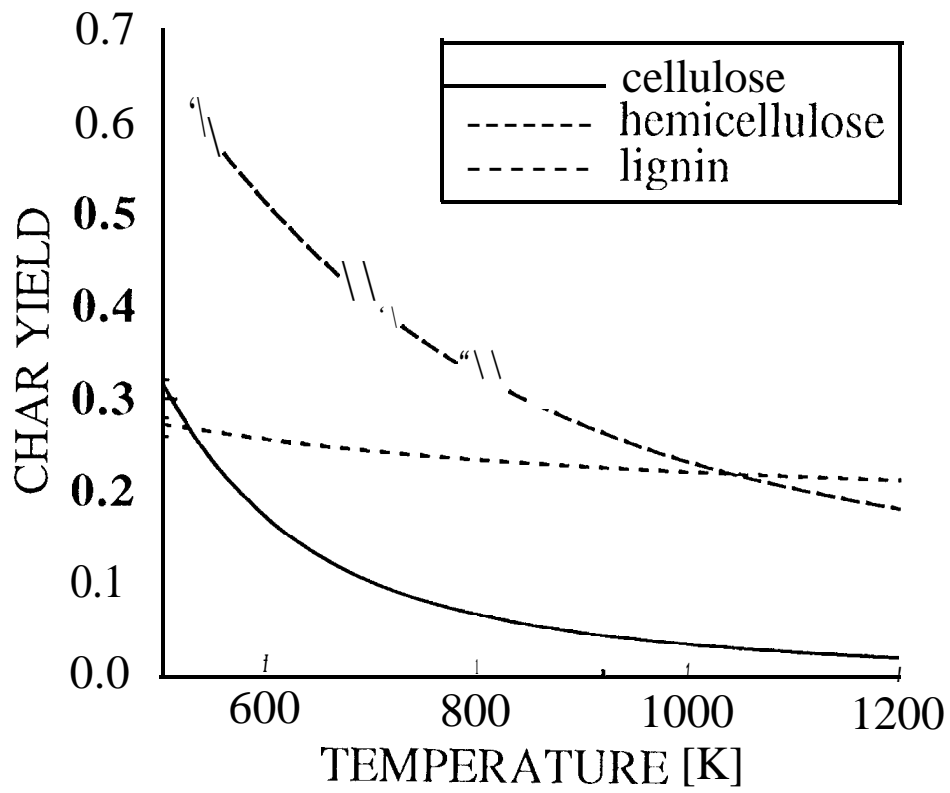


Figure 2

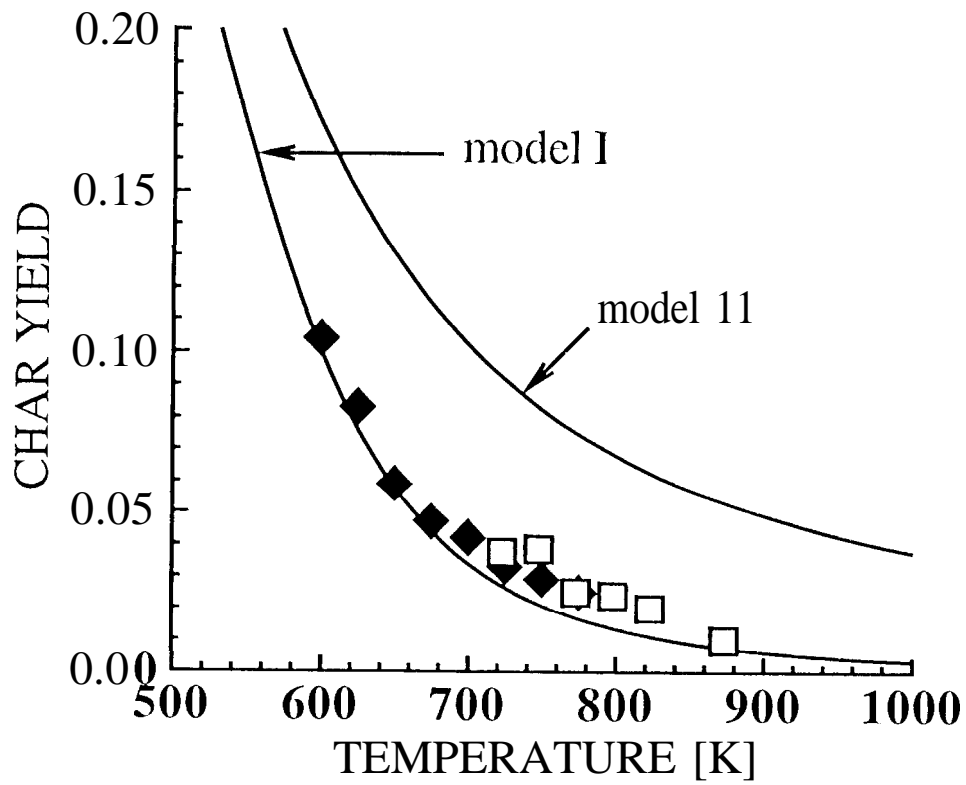


Figure 3

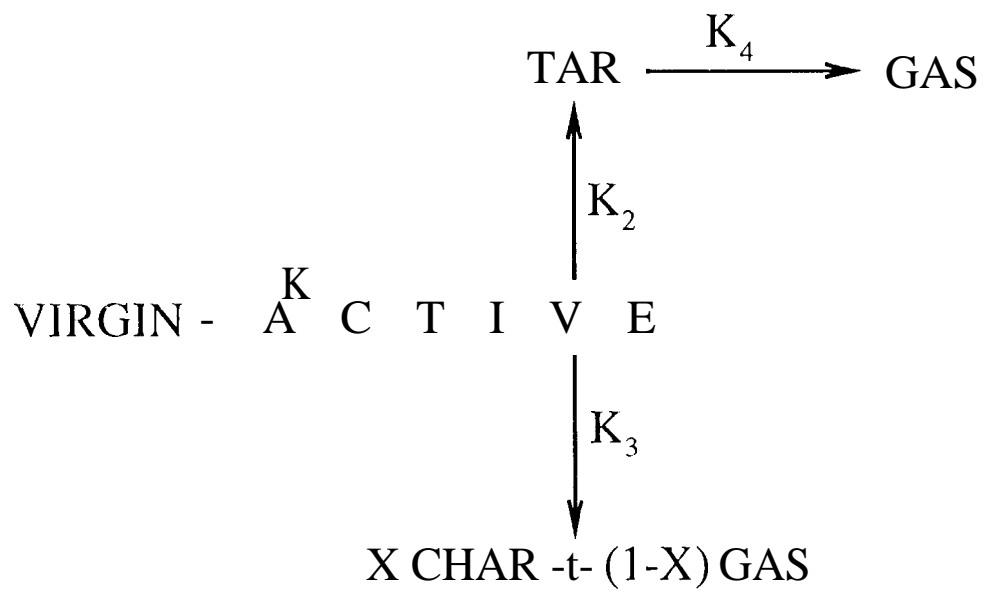


Figure 4

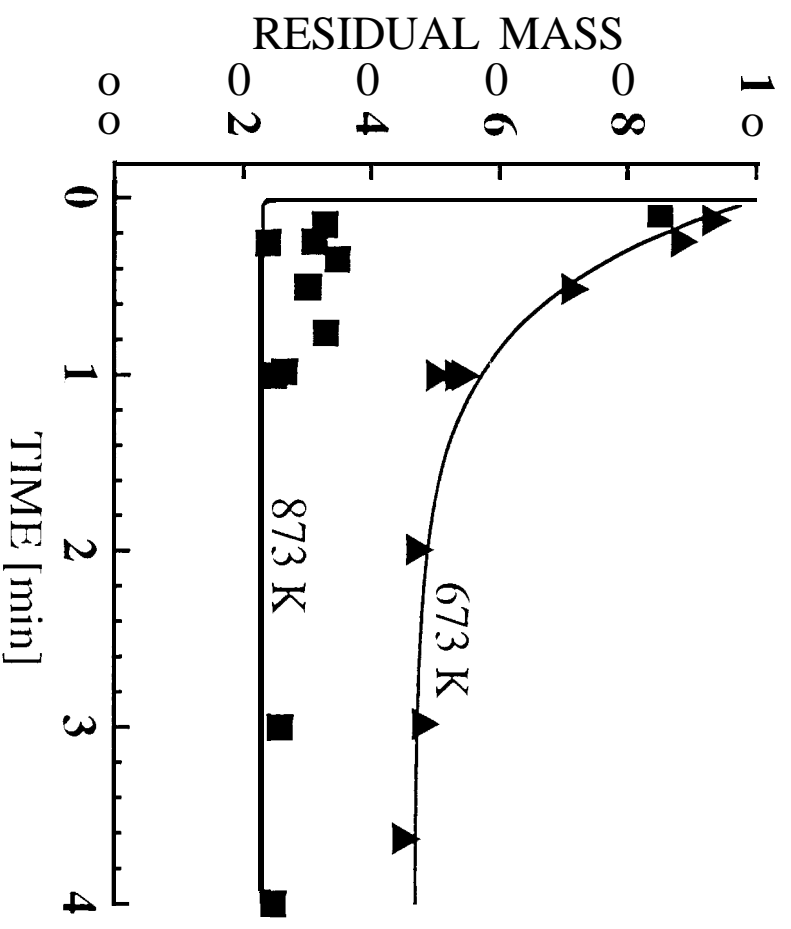


Figure 5

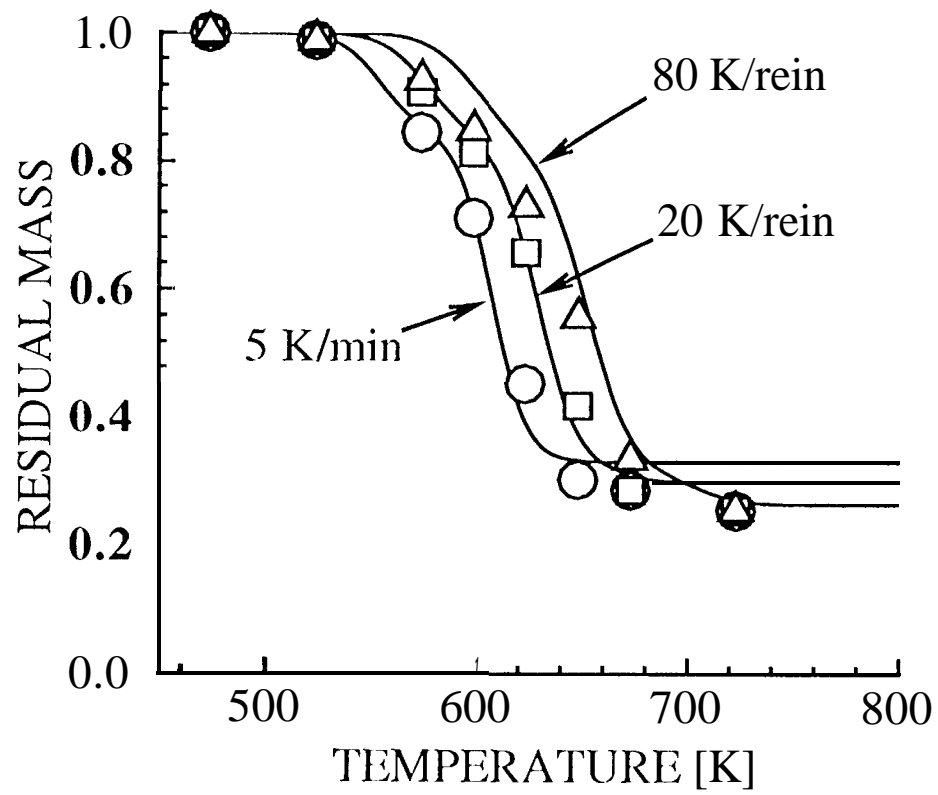


Figure 6

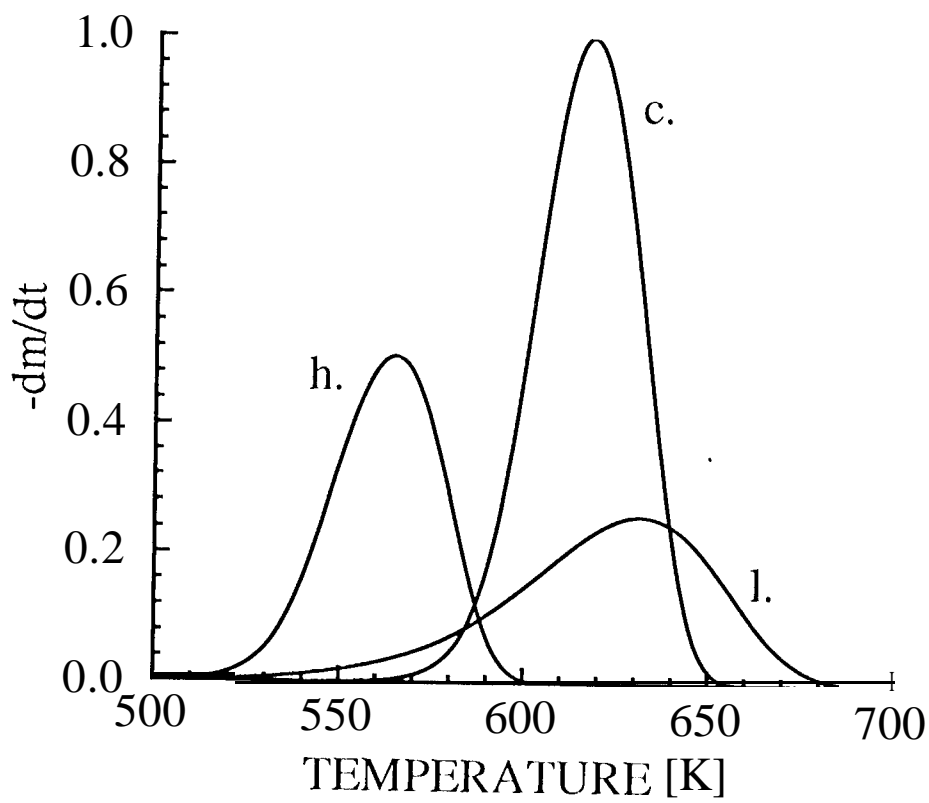


Figure 7

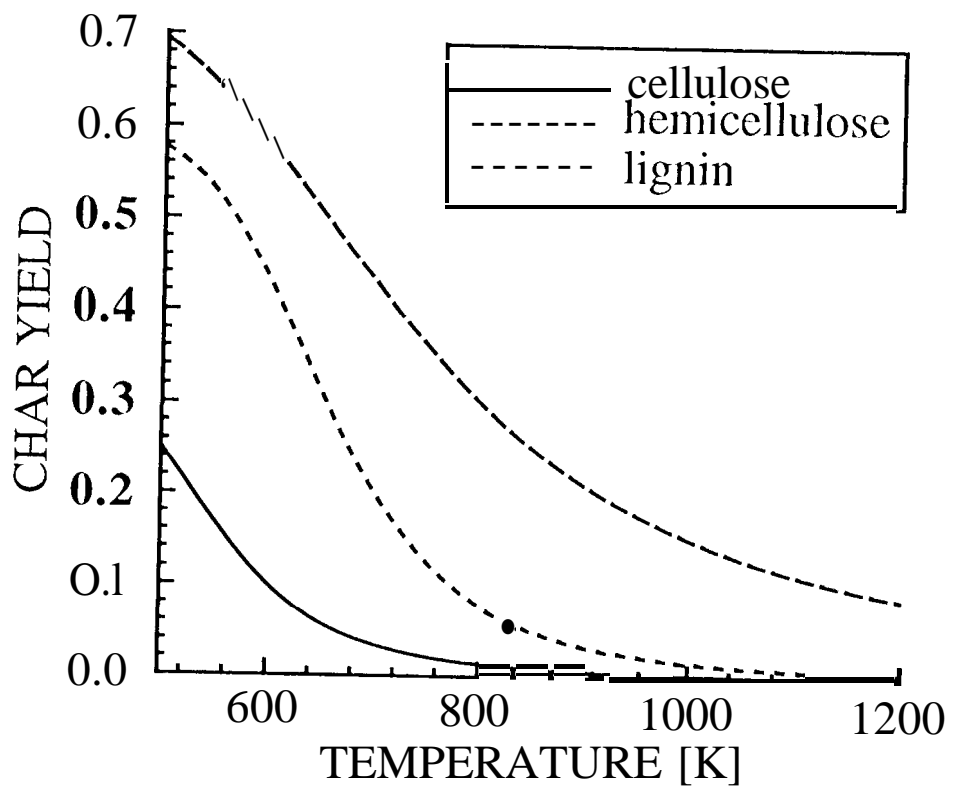


Figure 8

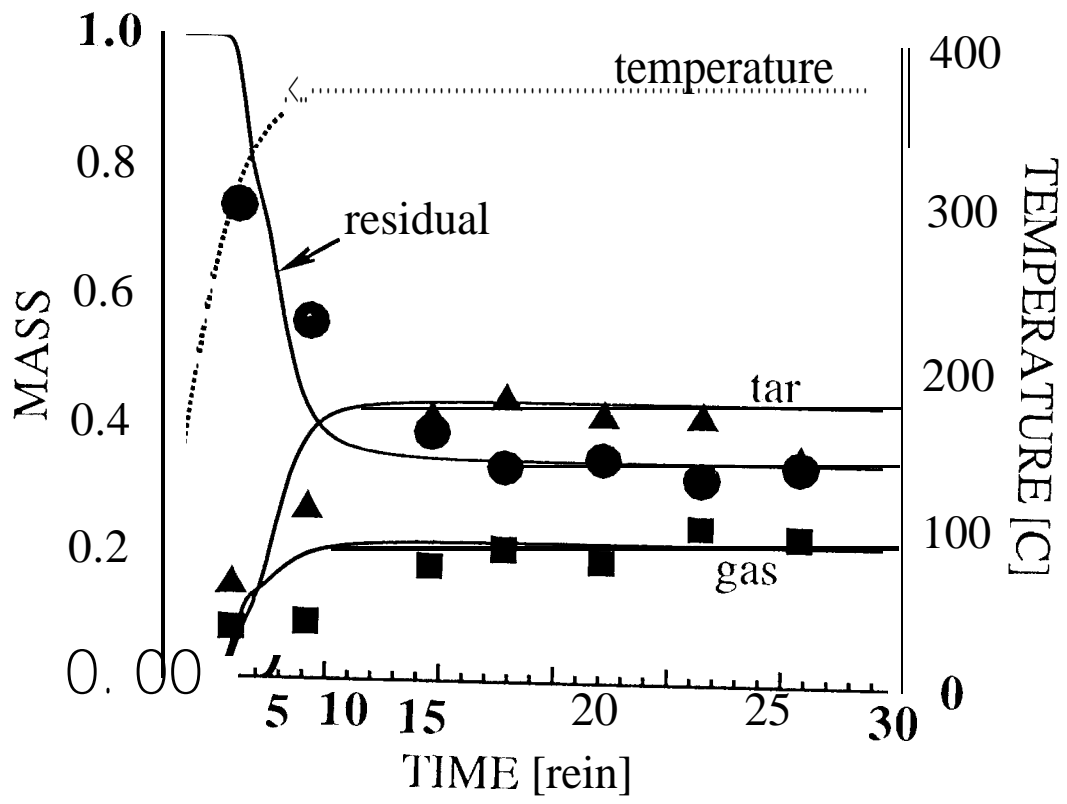


Figure 9

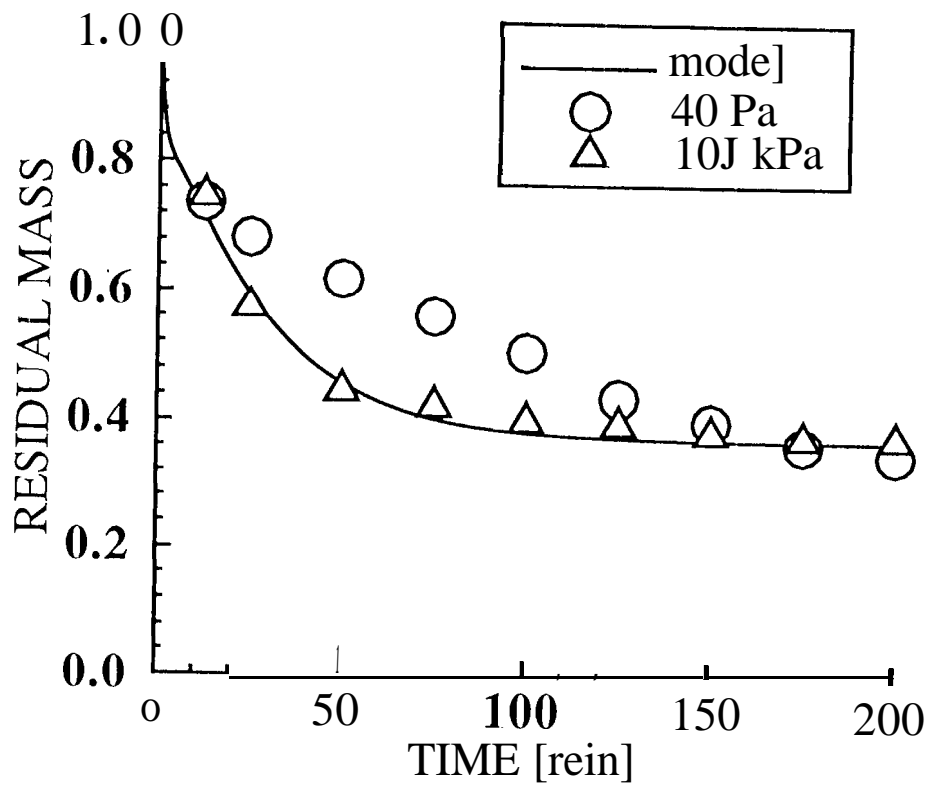


Figure 10

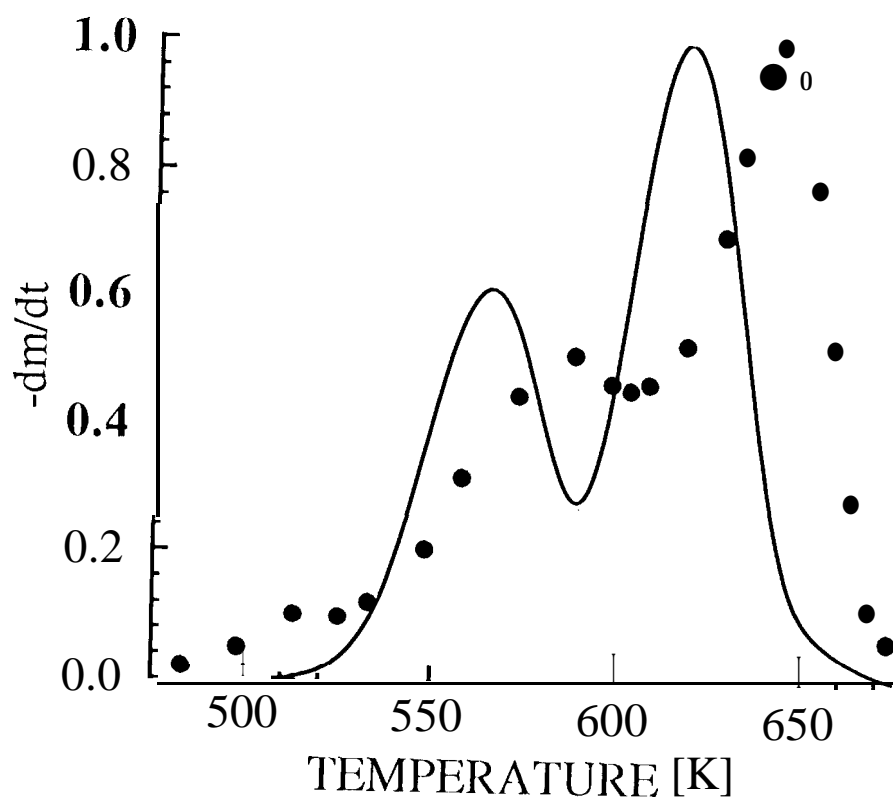


Figure 11

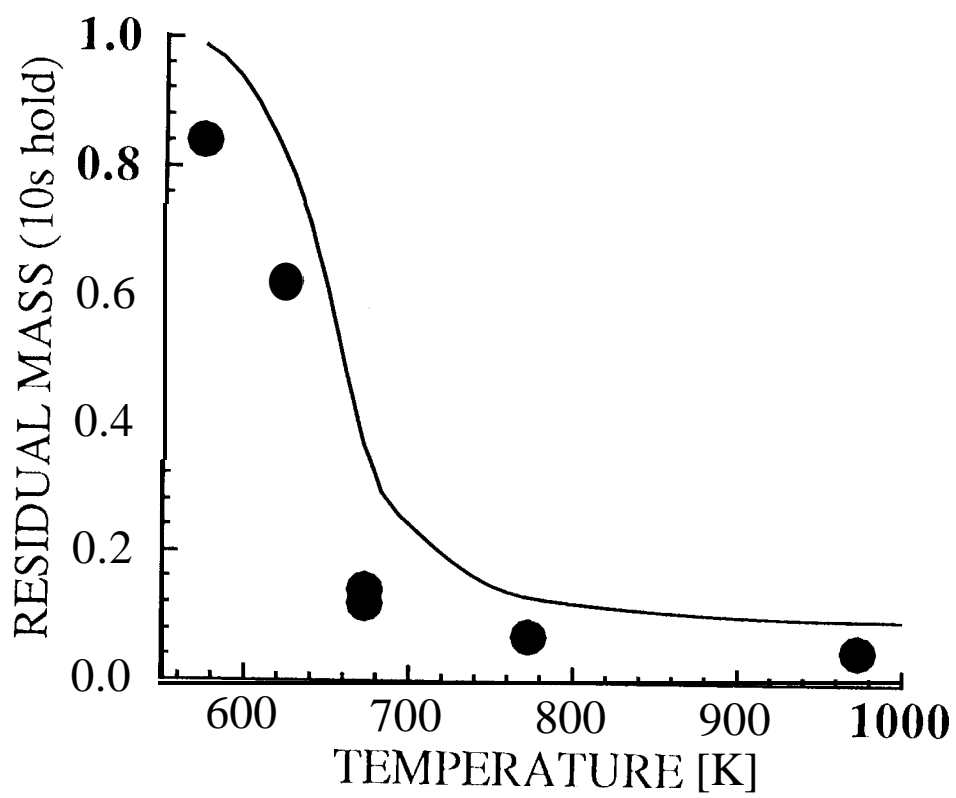


Figure 12

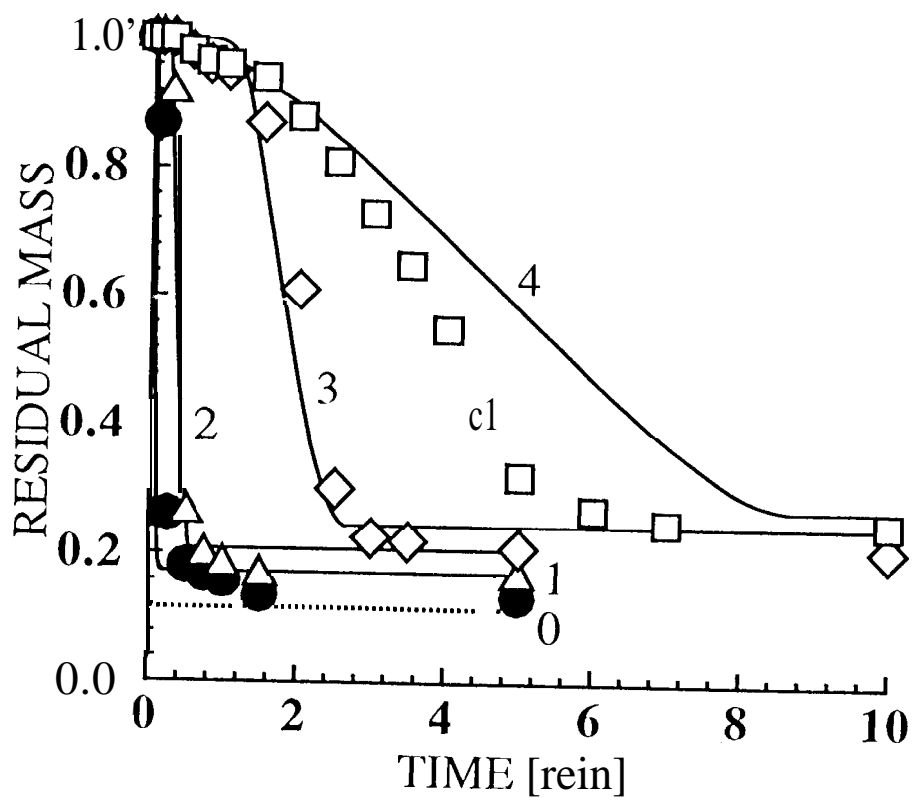


Figure 13

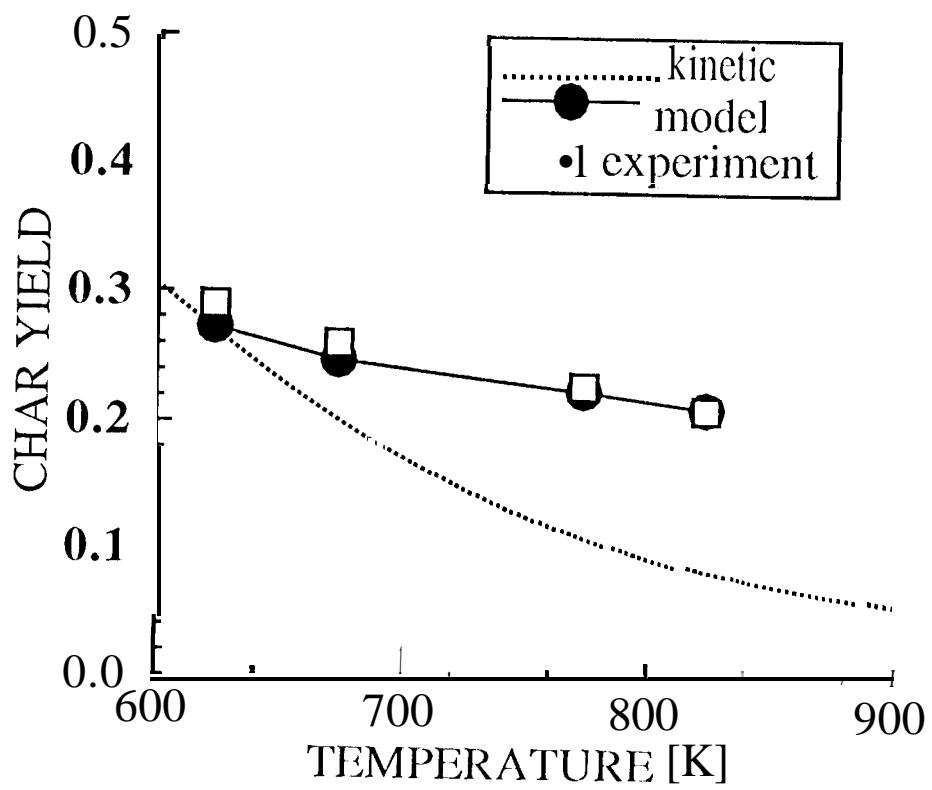


Figure 14(a)

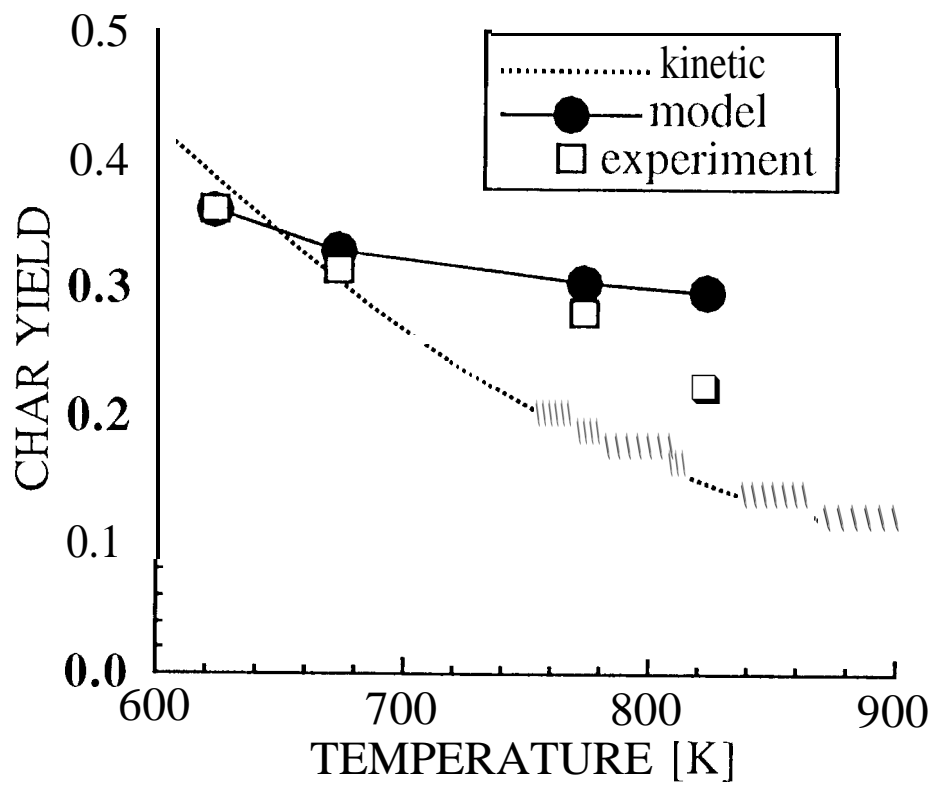


Figure 14 (b)

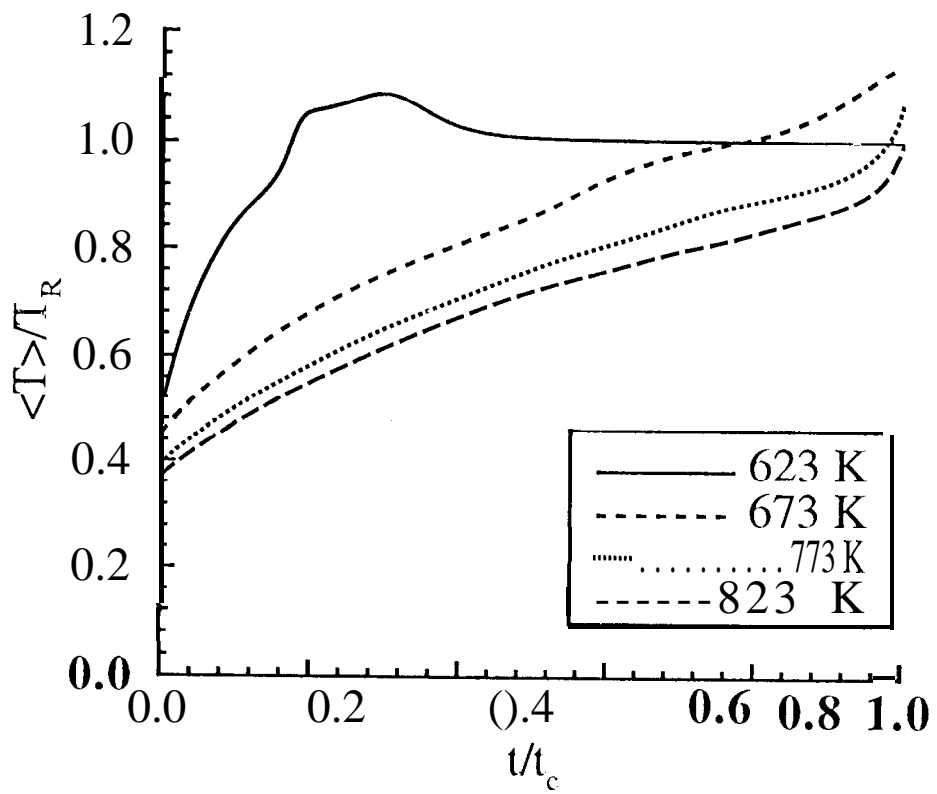


Figure 15

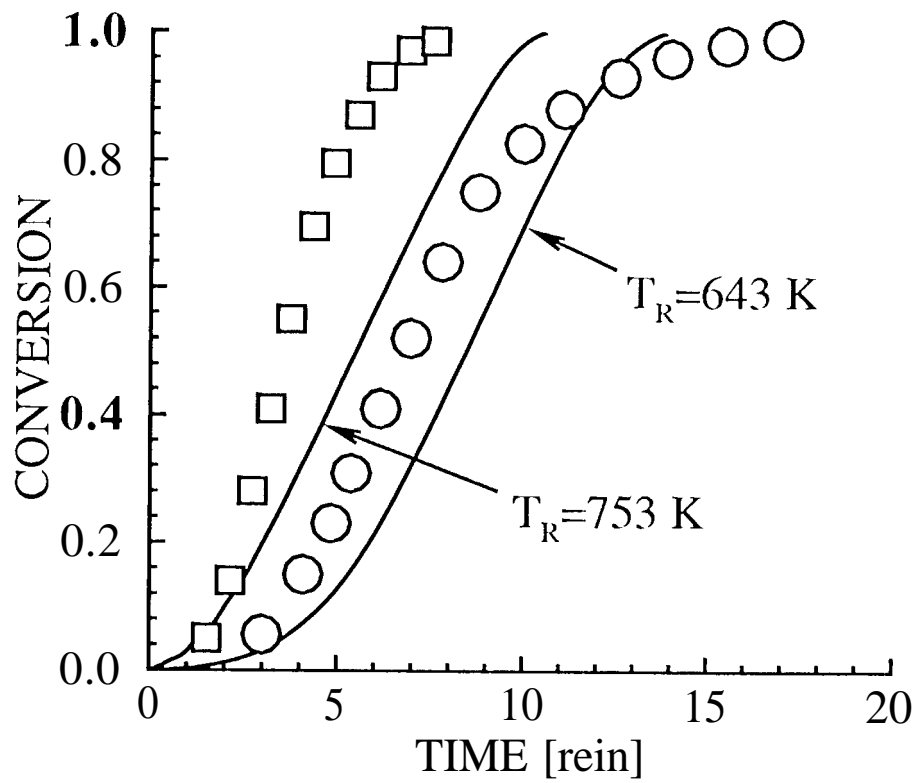


Figure 16

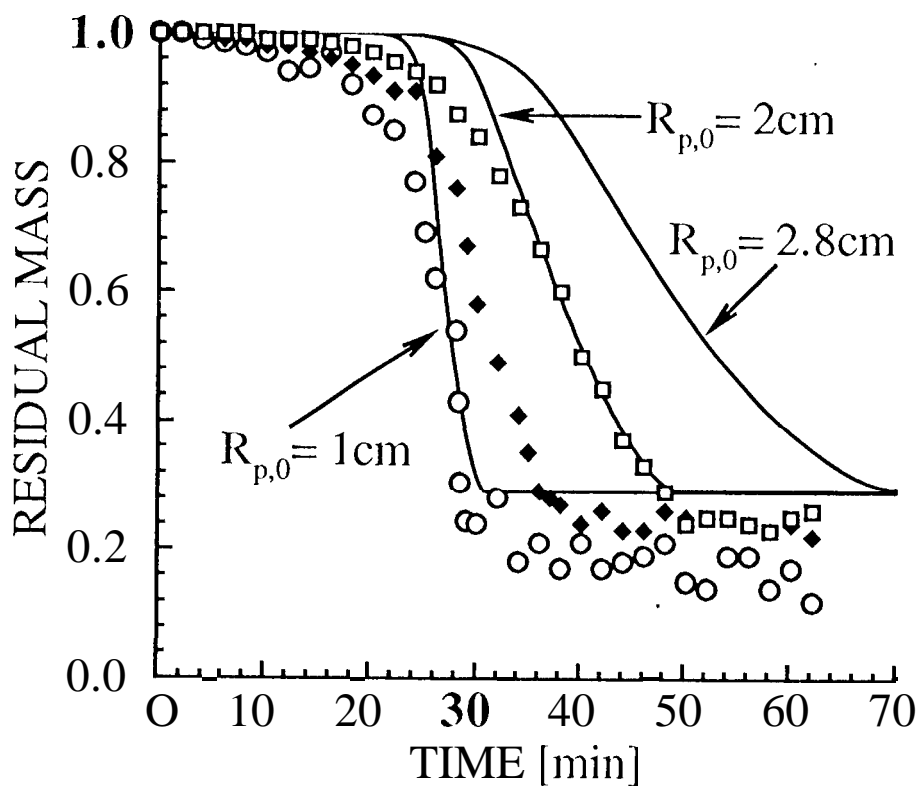


Figure 17

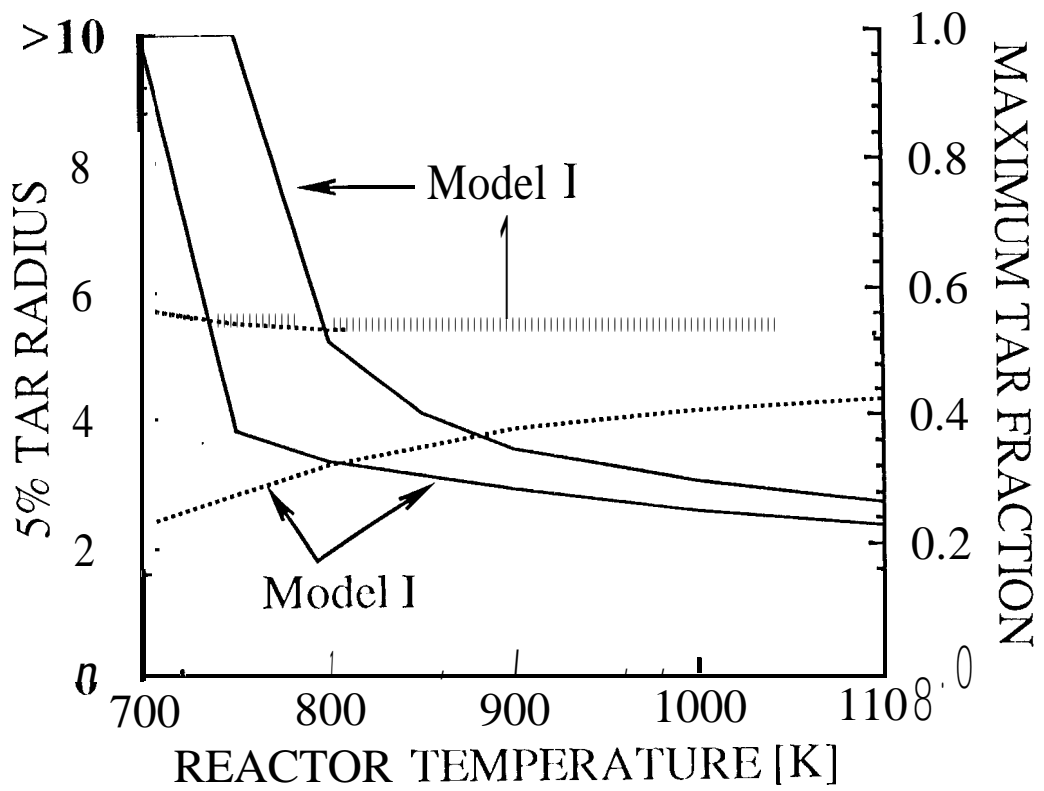


Figure 18